Electronic Theses and Dissertations   Theses, Dissertations, and Major Papers

9-9-2019

Effect of Plasma Electrolytic Oxidation Coating on Tensile Properties of High Pressure Die Cast Magnesium Alloy AZ91

Zixi Sun
University of Windsor

Follow this and additional works at: https://scholar.uwindsor.ca/etd

Recommended Citation

Effect of Plasma Electrolytic Oxidation Coating on Tensile Properties of High Pressure Die Cast Magnesium Alloy AZ91

By

Zixi Sun

A Thesis

Submitted to the Faculty of Graduate Studies

through the Department of Mechanical, Automotive and Materials Engineering

in Partial Fulfillment of the Requirements for

the Degree of Master of Applied Science

at the University of Windsor

Windsor, Ontario, Canada

2019

Effect of Plasma Electrolytic Oxidation Coating on Tensile Properties of High Pressure Die Cast Magnesium Alloy AZ91

by

Zixi Sun

APPROVED BY:

_____

M. Wang

Department of Mechanical, Automotive and Materials Engineering

_____

X. Nie

Department of Mechanical, Automotive and Materials Engineering

_____

H. Hu, Advisor

Department of Mechanical, Automotive and Materials Engineering

September 9th, 2019

DECLARATION OF CO-AUTHORSHIP / PREVIOUS PUBLICATION

I.   Co-Authorship

I hereby declare that this thesis incorporates material that is result of joint research, as follows:

In all cases, the key ideas, primary contributions, experimental designs, data analysis and interpretation, were performed by the author, Dr. H. Hu as advisor and Dr. X. Nie as co-advisor. Chapter 3, 4 and 5 were co-authored with Xinyu Geng and Luyang Ren. Xinyu Geng and Luyang Ren contributed in bulk samples preparations. I certify that, with the above qualification, this dissertation, and the research to which it refers, is the product of my own work.

I am aware of the University of Windsor Senate Policy on Authorship and I certify that I have properly acknowledged the contribution of other researchers to my thesis and have obtained written permission from each of the co-author(s) to include the above material(s) in my thesis.

I certify that, with the above qualification, this thesis, and the research to which it refers, is the product of my own work.

II.   Previous Publication

This thesis includes 3 original papers that have been previously published/submitted for publication in peer reviewed journals, as follows:

Thesis Chapter	Publication title/full citation	Publication status*
Chapter [3]	Zixi Sun, Luyang Ren, Xinyu Geng, Li Fang, Xingyuan Wei and Henry Hu, *Influence of Wall Stocks on Mechanical Properties of HPDC AZ91*	*Key Engineering Materials* *ISSN: 1662-9795, Vol. 793, pp41-45* *Published*
Chapter [4]	Zixi Sun, Xinyu Geng, Luyang Ren, and Henry Hu, *Microstructure, Tensile Properties and Fracture Behavior of HPDC Magnesium Alloy AZ91*	*2019 International Conference on Functional Materials and Applied Technologies* *Submitted*
Chapter [5]	Zixi Sun, Xinyu Geng, Luyang Ren, and Henry Hu, *Effect of PEO Coating on Tensile Properties of HPDC Magnesium Alloy AZ91*	*Prepared for submission*

I certify that I have obtained a written permission from the copyright owner(s) to include the above published material(s) in my thesis. I certify that the above material describes work completed during my registration as a graduate student at the University of Windsor.

III.   General

I declare that, to the best of my knowledge, my thesis does not infringe upon anyone's copyright nor violate any proprietary rights and that any ideas, techniques, quotations, or any other material from the work of other people included in my thesis, published or otherwise, are fully acknowledged in accordance with the standard referencing practices. Furthermore, to the extent that I have included copyrighted material that surpasses the bounds of fair dealing within the meaning of the Canada Copyright Act, I certify that I have obtained a written permission from the copyright owner(s) to include such material(s) in my thesis.

I declare that this is a true copy of my thesis, including any final revisions, as approved by my thesis committee and the Graduate Studies office, and that this thesis has not been submitted for a higher degree to any other University or Institution.

ABSTRACT

Magnesium alloy AZ91 is high pressure die cast (HPDC) into rectangular coupons with the section thicknesses of 2, 6 and 10 mm. The first group of samples is employed to investigate the effect of section thicknesses on tensile properties, strain-hardening and fracture behaviours of the die cast AZ91. The results of tensile testing indicate that the ultimate tensile strength (UTS), yield strength (YS), elongation (e_f), modulus(E), toughness(U_t) and resilience(U_r) decrease to 129.17, 110.59 MPa, 0.37%, 25.9 GPa, 0.89 MJ/m^3, and 236.10 kJ/m^3 from 245.54, 169.26 MPa, 4.07%, 37.8 GPa, 8.34 MJ/m^3, and 378.95 kJ/m^3 with increasing the section thicknesses of die cast AZ91 to 10 mm from 2 mm, respectively. The analysis of true stress vs. strain curves shows that the straining hardening rates increases with decreasing the section thickness to 2 mm from 10 m. The analyses of scanning electron microscopy (SEM) reveal that the high tensile properties of the HPDC Mg alloy AZ91 with the thin section thickness should be attributed to the low porosity level, fine dendrite structure, high eutectic content, and relatively thick skin. The observation via SEM fractography illustrates that the fracture behaviour of die cast AZ91 is influenced by section thicknesses. As the section thickness increases, the fracture of AZ91 tends to transit from ductile to brittle mode due to arising porosity content and coarsening microstructure. The second group of samples is employed to study the effect of plasma electrolytic oxidation (PEO) coating on tensile properties of the HPDC Mg alloy AZ91. The tensile test results show that the PEO coating reduces the UTS and YS of the 2 and 6 mm samples, but slightly enhance the tensile properties of 10 mm sample. The SEM analysis reveals that the differences in the size and content of pores between the substrate and the ceramic coating should be responsible for the change in the tensile properties.

DEDICATION

I dedicate this thesis to My Dear Mother,

Lizhen Ye

For Her Endless Love and Support,

without her I would have not been at where I am today.

ACKNOWLEDGEMENTS

■

Light weight metals have become one of the most desirable and necessary materials in the automotive and manufacture industries where lightweight structure is highly demanding. Their properties like high strength-to-weight ratios, good ductility and low density become new favorite in enhancing fuel efficiency. The use of magnesium in the automotive industry has grown dramatically in response to consumer demands for increased performance and fuel economy of vehicles. Magnesium is the eighth most common element in the earth's crust. Pure magnesium has a density of 1.7g/cc, which is 35% lower than aluminum and 78% lower than iron. Moreover, magnesium alloys offer not only light weight, but moderate mechanical properties. Thus, they provide to engineering designers a great choice for lightweight structural applications in the aerospace and automotive industries.

In the automotive industry, the most common manufacturing method is high pressure die casting (HPDC) to form parts of magnesium alloys. High pressure die cast magnesium alloys have a relatively good strength and high ductility at room temperature. Applications of HPDC magnesium alloys AZ91 include front end support assemblies, steering wheel armatures, steering column support brackets, door inner, tailgate, bulk head, instrument panel and engine cradle which have cross sections with difference thickness and complex shapes. HPDC processes are capable of casting of complex thin walled components with good surface finish and dimensional tolerance at very competitive prices. Understanding the effect of thick wall stocks on mechanical behaviors of HPDC AZ91 is crucial for proper design of lightweight components to meet desired

engineering requirement. Like all other metallic materials, there is also a trade-off in using magnesium alloys. Pure magnesium and magnesium alloys have poor corrosion resistance that greatly limits the expansion of their applications. The application of surface treatment can expand the field of applying magnesium alloys.

Plasma Electrolytic oxidation (PEO) process is an emerging, environmentally-friendly surface engineering technique to deposit ceramic coatings on magnesium and magnesium alloys for corrosion protection. Throughout years, researchers have developed the chemical compositions of electrolyte and PEO process parameters for corrosion prevention of magnesium alloys. The results show PEO can significantly improve corrosion resistance of magnesium alloys. In the open literature, however, little information is available on PEO coating effect on the mechanical properties of HPDC magnesium alloys with different section thicknesses.

■■ ■■■■■■■■■■■■

The objectives of this work are outlined as follow:

- Evaluate the tensile properties of high pressure die cast magnesium alloy AZ91 with section thicknesses of 2, 6 and 10 mm;

- Investigate the microstructure of high pressure die cast magnesium alloy AZ91 with three different section thickness;

- Analysis the effect of section thickness on mechanical properties of AZ91;

- Apply PEO coating on surface of HPDC AZ91 alloy and conduct the tensile test;

- Investigate the microstructure of the PEO ceramic layer and substrate of HPDC AZ91 alloy;

- Compare the mechanical properties of PEO coated and uncoated HPDC AZ91 alloy with three section thicknesses; and

- Determine the effect of PEO coating on mechanical properties of HPDC AZ91 alloys with different section thicknesses.

■■   ■■■■■■■■■■■■

  This thesis contains six chapters. Chapter 1 provides a general background of high pressure die cast and plasma electrolytic oxidation process, and the objectives of this study. Chapter 2 provides the literature review about the investigation in the process of high pressure die casting, the metallurgical aspects of magnesium alloy AZ91, the mechanism and process of PEO coating. Chapters 3 and 4 report the results of the effects of section thickness on tensile behaviors and microstructure of high pressure die cast magnesium alloy AZ91. In Chapter 5, the effect of PEO coating on mechanical properties of HPDC AZ91 alloy with different section thicknesses is discussed. Chapter 6 concludes and summarizes the present study. Lastly, Chapter 7 presents the recommendations for future work.

2.1.1 Crystal structure of pure magnesium

Magnesium has a hexagonal close-packed structure (hcp) constituted by lattice dimensions of c=5.199A and a=3.202A. The axial ration c/a= 1.6237 is close to the theoretical Close-packing c/a=1.633, which is obtained for incompressible spheres. Magnesium is the only hcp metal that has an atom that approaches true spherical shape [1].

2.1.2 Alloying Elements in Magnesium Alloy AZ91 and Their General Effects

Pure magnesium has low mechanical properties. Like other structural metals, such as Al, Zn or Fe, magnesium has to be alloyed for the improvement of its overall mechanical properties and the activation of the matter for engineering applications. A summary of the effect of some alloying elements and their effect on the metallurgical behavior of magnesium are provided below for references [1-3]:

Aluminum: Al has a maximum solubility of 12.7 wt% in magnesium at the eutectic temperature. It confers strength and refines the cast structure of magnesium, particularly in conjunction with superheating.

Manganese: Mn has a solubility of 2.2 wt% at the peri-tectic temperature. It forms the basis for the well established medium strength Mg-Mn wrought alloys and the more recent Mg-Al-Mn pressure die casting alloys. Mn is added to AZ91 alloy in small quantities (0.4 wt%) mainly to improve the corrosion resistance of the alloy. It transforms

FeAl$_3$ into (FeMn) Al$_6$ intermetallics and thus eliminates the problematic electrolytic potential difference between the impurity iron compound and the Mg matrix [4].

Zinc: Zn has a maximum solubility of 6.2 wt% at the eutectic temperature. It causes grain refinement and increase of strength in Mg. Alloys containing Zn are heat treatable but are somewhat brittle and prone to hot shortness unless Zn is added to further refine the grain size.

2.1.3   Effect of Al and Zn on the Mechanical Properties and Die Castability of Magnesium alloy

There are few literatures available concerning the individual effects of Al and Zn on the elongation or on the tensile properties of as-cast magnesium binary alloys. In the existing literatures, the properties reported are either for the heat treated or worked condition, neither of which truly represent the properties of the as-cast microstructure that are crucial data for present work. The earliest data is found in the work of Fox (1945) [5], which measures the tensile properties of as-cast Mg-Al and Mg-Zn sand cast alloys. Fox's results are demonstrated in Figures 2.1 and 2.2, specifically concerning the effect of Al and Zn on ultimate tensile strength (UTS), proof stress (yield) and elongation [5]. In Mg-Al alloys, the UTS and elongation achieve a maximum at 4 and 6 wt% Al respectively and then decrease, while proof stress (yield) increases monotonically up to 12 wt% Al. In Mg-Zn alloys, the UTS shows a peak at 6%Zn, while elongation shows a decreasing trend after 4wt% Zn. The proof stress also increases monotonically up to 12 wt% Zn.
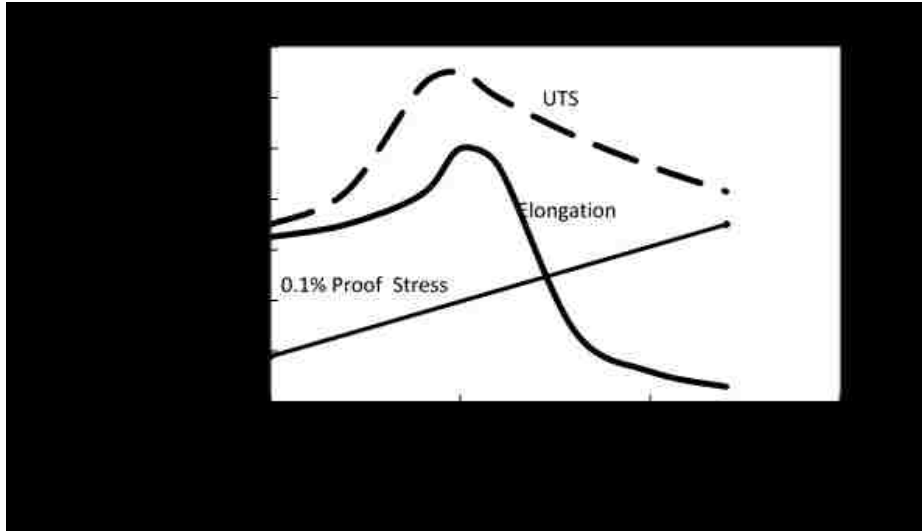
Figure 2.1 Tensile properties of sand cast (as-cast) Mg-Al alloys [5].
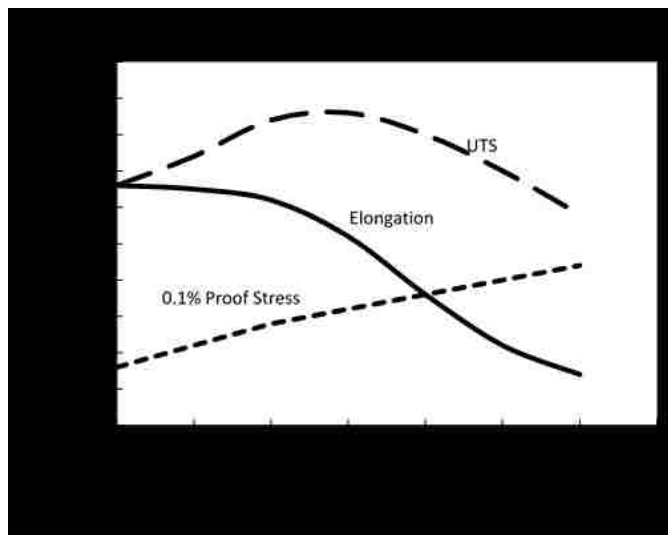
Figure 2.2 Tensile properties of sand cast (as-cast) Mg-Zn alloys [5].

2.1.4   Phase Diagram Considerations and Solidification of AZ91

Alloying additions to magnesium can change magnesium's structure, forming new phases. The mechanical properties of as-cast Mg alloys are strongly dependent on their microstructural features, including grain size, type, size and distribution of constitute phases and crystallographic direction (texture). In reference to the phase diagram, this

section presents and discusses the formation of phases during general solidification, growth directions and castability of AZ91.

Although AZ91 is actually a ternary alloy, it may be practically considered as being based upon the binary Mg-Al system. The Mg-Al binary phase diagram, which is most widely accepted, is displayed as Figure 2.3 [6].
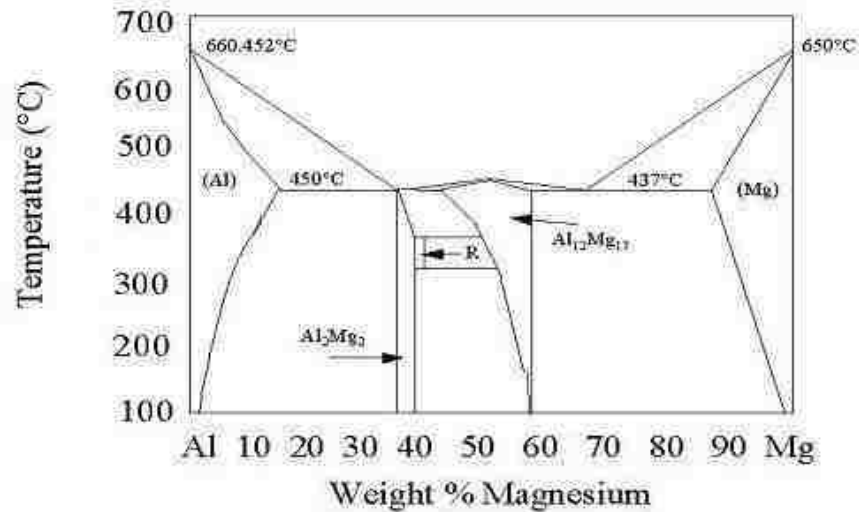
Figure 2.3 The Al-Mg binary equilibrium phase diagram [6].

Significant academic interests have been placed at the Mg-rich portion of the equilibrium phase diagram, because AZ91 is based around the composition Mg-9 wt%Al. The solidus line on the Mg-rich side shows a decreasing solid solubility of Al from 12.7wt% at 437^0C to 3.2 wt% at 204 ^{0}C, indicating that Mg-Al alloys are likely to be age-hardened. When the solubility of Al exceeds 12.7 wt%, an intermetallic phase of stoichiometric composition $Mg_{17}Al_{12}$ is formed as an eutectic, with a melting point of 437 ^{0}C. The structure of $Mg_{17}Al_{12}$ based on the ideal composition (58.62 wt% Mg) is suggested to be an α-Mg type cubic unit cell consisting of 58 atoms [7]. The lattice

7

constant of the intermetallic compound varies linearly between 10.469Å at 51.6wt%Mg to 10.591 Å at 61.5wt% Mg [7].

According to the reviewed literatures, the formation of β-$Mg_{17}Al_{12}$ phase is inevitable when AZ91 is cast by high pressure die casting processes. The volume fraction, shape and size of β-$Mg_{17}Al_{12}$ influence the mechanical properties of die cast or squeeze cast AZ91. Present literatures have not identified if die cast or squeeze cast AZ91 also exhibits any preferential growth direction. This preferential growth can be expected to result in anisotropic mechanical properties. Moreover, in die cast AZ91 parts, porosity formation may be influenced by the relatively high eutectic content and its final solidification. In sand cast Mg-Al alloys, microporosity is found to associate with "low melting point constituent" or eutectic [8], confirming imperfect feeding as a major cause of microporosity.

2.2.1   Die Casting Process

The presently employed die casting process typically utilize high pressure die casting (HPDC), a process of which used to produce complexly shaped non-ferrous metal parts by large quantities. Such a process is highly mechanized, first-high-cost, with high production rate. The HPDC is first-high-cost because it requires permanent mold dies using metals like H13 steel, which is highly expensive, making it economical only for high volume castings [9]. Two kinds of HPDC machines, including the hot chamber and cold chamber variations, are shown below in Figures 2.4 and 2.5 [10,11].
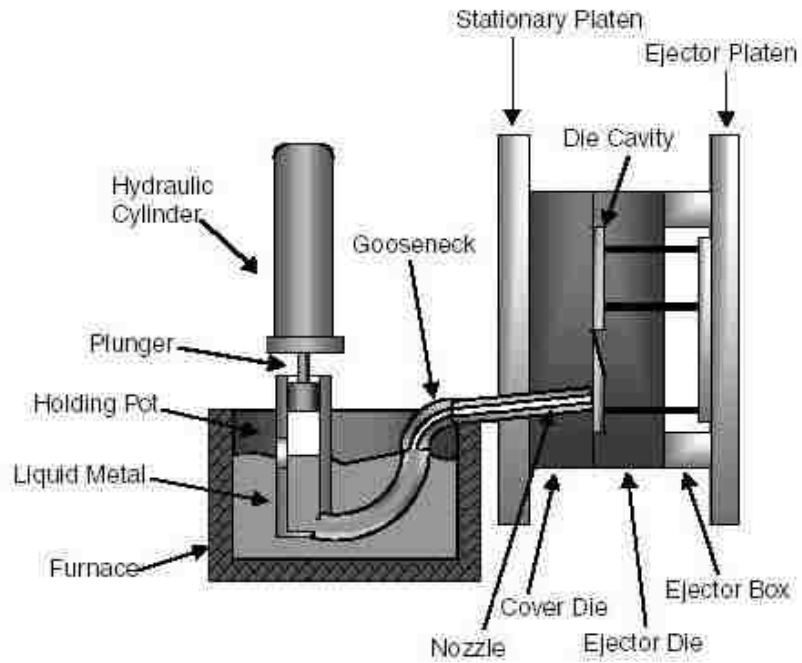
Figure 2.4 Schematic diagram of a hot-chamber die casting machine [11].
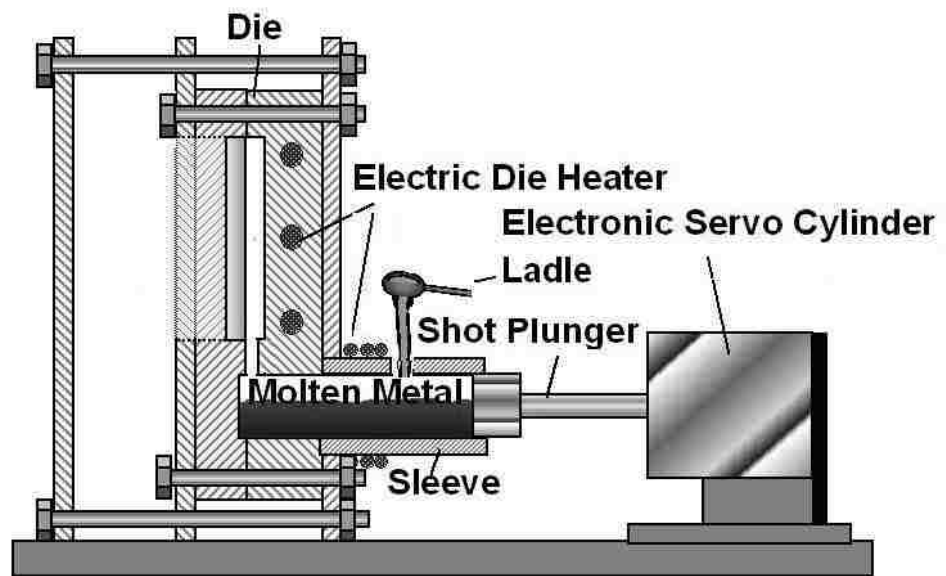
Figure 2.5 Schematic diagram of cold chamber die casting machine [10].

2.2.2 Cold chamber die casting

A cold chamber die casting process consists of the following steps:

1. Die is closed and molten metal is ladled into the cold chamber cylinder;

2. Plunger pushes molten metal into die cavity. The metal is held under high pressure until it solidifies;

3. Die opens and plunger follows to push the solidified slug from the cylinder. Cores, if any, retract; and

4. Ejector pins push casting off ejector die and plunger returns to its original position[10].

2.2.3 Hot chamber die casting

A hot chamber die casting process involves:

1. Die is closed and gooseneck cylinder is filled with molten metal;

2. Plunger pushes molten metal through gooseneck passage and nozzle and the cavity. Metal is held under pressure until it solidifies;

3. Die opens and cores, if any, retract. Casting stays in ejector die. Plunger returns, pulling molten metal back through nozzle and gooseneck; and

4. Ejector pins push casting out of ejector die. As plunger uncovers inlet hole, molten metal refills gooseneck cylinder.

Figure 2.5 schematically shows the commonly used hot chamber die casting machine [11].

Comparing to other manufacturing techniques, high pressure die casting stands out in its production efficiency and economic value, as well as capacity to produce a variety of

components in different shapes. Parts produced by die casting also have long service life, in addition to the quality of easily fitting to the surround parts. The advantages of die casting in detail are presented as the following:

High-speed production – die casting provides more complexity in shapes within closer tolerances than most other mass production processes, with little to no requirement for machining. Additionally, thousands of identical castings can be produced before additional tooling is required.

Dimensional accuracy and stability – die casting produces parts with higher durability, dimensional stability, and heat resistance than, while achieving the same level of close tolerance as conventional sand casting.

Strength and weight – die cast parts are stronger than plastic injection moldings with the same dimensions. Thin wall castings are stronger and lighter than that produced by any other casting methods. Further, products of die casting's strength depend on the alloy rather than the joining process, since die castings does not consist of separate parts welded or fastened together.

Multiple finishing techniques – die cast parts can be produced with smooth or textured surfaces, making them easily plated or finished with a minimum of surface preparation.

Simply assembly – die castings provide integral fastening elements, such as bosses and studs, which allows simple process in assembly. Holes can be cored and made to tape drill sizes, or external treads can be cast [12].

2.3.1 Origin of Porosity in Die Castings

There are four main causes of porosity in any die casting [13]:

1. Shrinkage porosity due to differences in specific volumes of the molten metal at the liquidus temperature and the solidified metal at the solidus temperature;

2. Release of dissolved hydrogen during the solidification and its subsequent entrapment;

3. Porosity due to vaporization of die lubricant and die spray; and

4. Trapped air arising in the die casting process.

2.3.2   Die Cast Microstructure and Properties

Literatures [14-17] on the microstructure and properties evolution of high pressure magnesium alloy die castings are relatively abundant. The work of Haavard et al [14] studies typical die cast magnesium alloy AZ91D and AM50 with 1, 3 and 9 mm section thicknesses, and also investigates the influence of cooling rate on microstructure and mechanical properties. The mechanical properties of magnesium alloys are found to be strongly affected by grain size. Smaller grain size helps to improve ductility and strength of castings, whereas thicker wall reduces mechanical strength and ductility [21]. On the other hand, Mao [15] reports the results of tensile tests on die cast AZ91D and AM60B magnesium alloy, as well as reverse bending fatigue tests on AM60B alloy, and observed relations between section size, porosity levels and the measured mechanical properties. In Wang et al's [16] work, the microstructure of AM50 magnesium alloys and the dislocation arrangement in the stressed states are examined through conventional transmission electron microscopy (TEM), high-resolution transmission electron microscopy (HRTEM), and energy dispersive X-ray (EDX) analysis. It has been found [17] that the deformation and fracture behavior of die cast AM50 and AM60 magnesium

alloys under examination shows fracture in bending and tension drawing inferences to the elucidation of the influences of microstructure and porosity on ductility.

Many past studies [18-24] reported that the tensile properties of cast magnesium-based alloys depend on the cross-sectional thickness of the casting and/or the distance from the mold surface of the part. Although the section thickness is an easily measurable parameter for comparing various castings, it may not be sufficient to predict the microstructure of the part and the associated mechanical properties. For example, it has been [20] proposed that the local solidification time is a more suitable parameter than the thickness of the section, and is used to predict the tensile properties of the cast component. Feinbeg et al. [21] showed that the mechanical properties of castings, such as ultimate tensile strength, tensile elongation at break and fatigue limit, are affected by the porosity of the component. The results presented by Sequeira et al. [24] show that the microstructure and mechanical properties change even when the cross-sectional thickness of the AZ91D high-pressure die casting changes under optimal casting conditions. When the section thickness is reduced, the yield strength and ultimate tensile strength is increased more than expected. In addition, changes in mechanical properties are observed in thick and thin die cast parts when the gate conditions are changed from the optimum setting. In terms of microstructure, solidification, wedge casting experiments and computer simulation of shot blasting sleeves, the mechanical properties of the best cast profiles vary with section thickness.

It has previously been shown that the formation of microstructures in high pressure die cast magnesium in cold chambers is carried out in two stages [25]. In the first stage, there is a growth of primary magnesium dendrites in the sleeve prior to

injection into the mold. Thus, the input material is actually a partially cured material with a solid fraction of up to about 20% solids [26]. This means that the metal injected into the mold from the spray sleeve contains a certain proportion of solids. Second, the resulting semi-solid slurry then enters the mold cavity through the narrow gate at high velocity. The flow of the semi-solid slurry through the narrow gate may affect the morphology of the solid portion that has been nucleated, thus affecting the final microstructure. Once the metal is filled with the die casting cavity, the pressure applied to the solidified casting by the piston causes intimate contact of the metal with the mold and produces a very high cooling rate (cooling rate in the range of 1000-10 $^\circ$ C / s). Therefore, the microstructure generated in cold chamber die casting is complex and subject to direct and indirect processing variables.

Figure 2.6 shows the tensile curves of die cast AZ91D alloy with different section thickness [14]. The tensile properties, the ultimate tensile strength (UTS), the yield strength (YS, 0.2% Proof stress) and elongation at fracture (e_f) of die cast AZ91D alloy are present in Figure 2.7 [14]. It is clear that the mechanical properties are decreasing with increasing thickness of the plates.
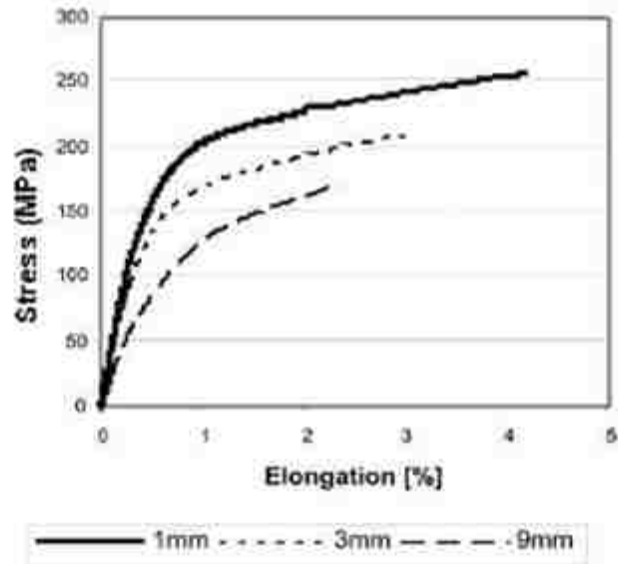
Figure 2.6 Tensile curves of die cast AZ91D with different section thickness [14].
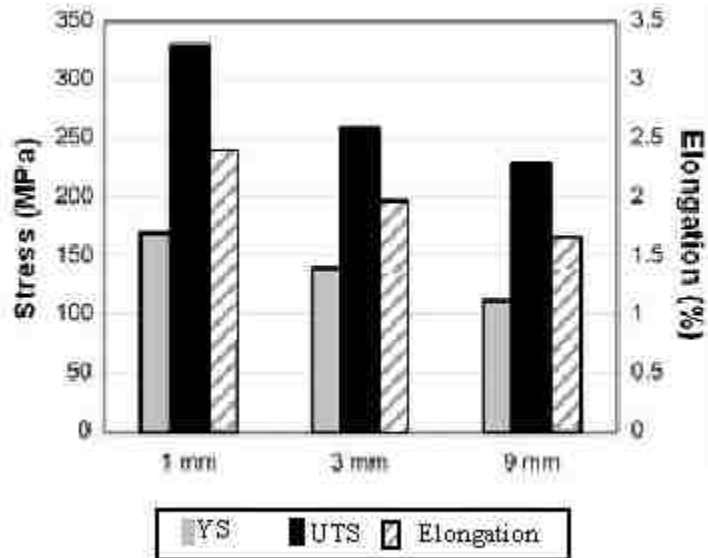
Figure 2.7 Tensile properties of die cast AZ91D with different section thickness [14].

2.4.1   Introduction of squeeze casting

Squeeze casting is a process involving the solidification of molten metal in a closed mold at an applied high pressure. Other terms used to describe the same or similar processes are liquid metal forging, squeeze casting, and pressure crystallization. The high applied pressure is several orders of magnitude higher than the melt pressure produced during normal casting, keeping the entrained gas in solution and squeezing the molten metal from the hot spot to the initial shrinkage hole. As a result, the porosity in the extruded cast part is almost eliminated. Furthermore, since the air gap at the liquid-liquid interface is eliminated by the applied high pressure, heat transfer on the surface of the mold is enhanced, which increases the solidification and cooling rates. Therefore, the excellent mechanical properties of the casting produced by the non-porous fine structure are achieved in the squeeze casting process [27].

2.4.2   Squeeze Casting Process

Squeeze casting bases on the principle of pressurized solidification, a process by which finished castings is able to be produced in a single process from molten metal to solid components within re-usable dies. Figure 2.8 shows the schematic diagram of a squeeze casting machine. The process which is schematically shown in Figure 2.9 involves several steps[28]:

1. A suitable dieset is installed on the bed of a hydraulic press. The dieset is preheated to a required working temperature. During the heating-up period, the dieset is usually sprayed with a commercial graphite lubricant;

2. A metered quantity of molten metal is poured into an open female die cavity. Then, an upper male die or punch is lowered, coming into contact with the liquid metal;

3. The pressure is applied shortly after molten metal begins to solidify and is maintained until all the molten metal has solidified;

4. The upper punch returns to its original position and the casting is ejected.

Overall, two different types of squeeze casting techniques have been developed based on different methods of metal metering and metal movement, referred to as "direct" and "indirect". Figure 2.10 is a schematic illustration of the direct and indirect modes of squeeze casting. Direct squeeze casting technology is characterized by direct pressure applied to the casting without any casting system, as shown in Figure 2.10. Since the pressure is applied directly to the entire surface of the molten metal during solidification, this technique provides a completely dense composition and extremely fast heat transfer, which results in a fine grain structure. As a result, higher mechanical properties are obtained. However, in the indirect technique shown in Figure 2.10 (b), pressure is applied to the load that transfers the load to the component.

Since pressure is applied at a distance from the component, it is difficult to maintain a high pressure on the component throughout the solidification and cooling. This indicates that it is difficult to cast an alloy of a long freezing range using indirect techniques. Moreover, due to the need to use a gating system, metal production is much lower than that achieved by direct squeeze casting. The advantage of indirect technology is that due to the presence of the gate system, a highly accurate external metering system is not required. Adjust the change in metal volume in the gate. While direct technology seems to offer more opportunities for a variety of alloys, it can be used to produce high-

strength, complete metal castings and metal-based composite parts. This is the concept of squeeze casting, and more indirect squeeze casting machines are currently in operation.This may be because the indirect process has been successfully commercialized.
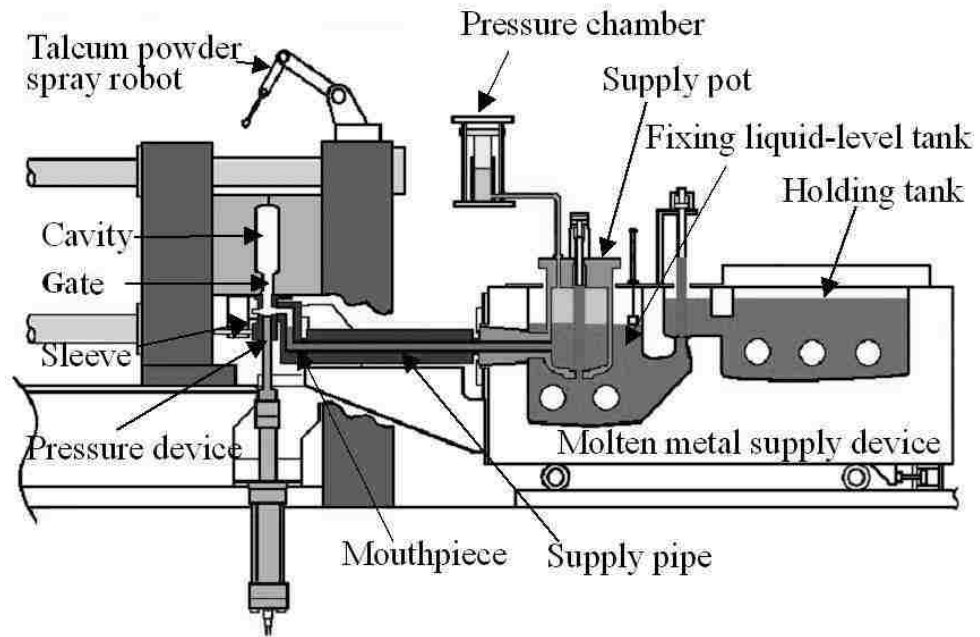
Figure 2.8 Schematic diagram of squeeze casting machine [29]

PUNCH

CRUCIBLE →

DIE

EJECTOR
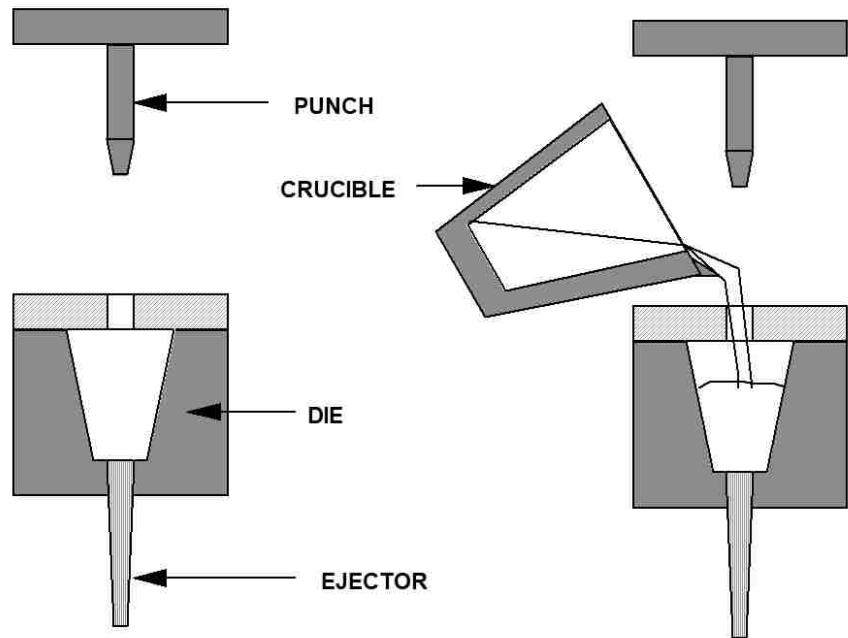
STEP 1: Preheat, Lubricating tooling.   STEP 2: Transfer melt into die cavity.
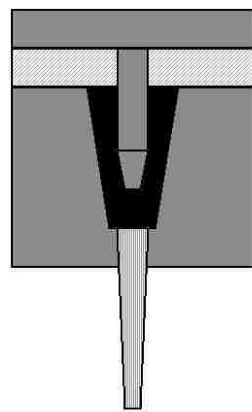
STEP 3: Solidify melt under pressure.   STEP 4: Eject casting.
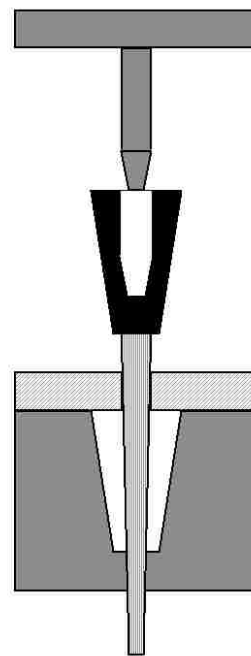
Figure 2.9 Schematic diagram of squeeze casting process [27].

19

(a)   (b)
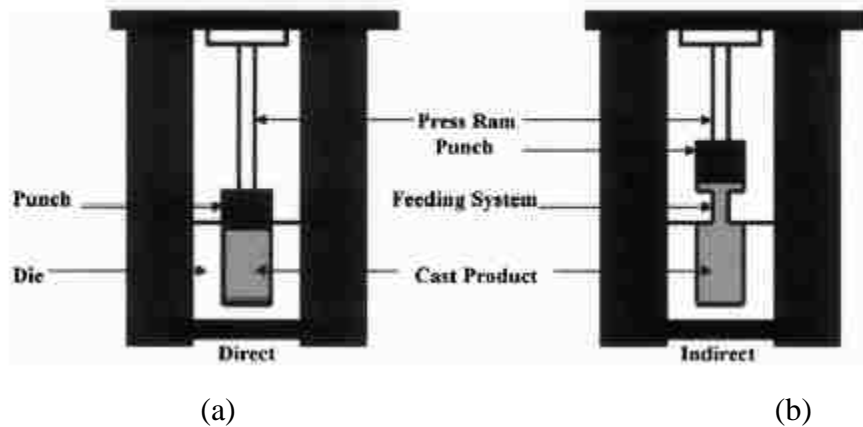
Figure 2.10 Schematic diagram to illustrate the (a) direct and (b) indirect modes of the squeeze casting

process [28].

2.4.3   Squeeze Casting of Magnesium Alloys

There are many scholarly resources on aluminum alloy squeeze casting. Though the exploration of squeeze casting of magnesium and its alloys has still not been extensive, recent development in the aluminum casting industry has successfully managed to employ the squeeze casting process to produce diverse components.

In the past few years, some publications on magnesium alloy squeeze casting has emerged. As the most common magnesium casting alloy, the alloy AZ91 has been the focus of most of the researches. For example, Ha [30] studies three key parameters, namely the effect of pressure, mold temperature and casting temperature on the solidification behavior and microstructure of two different types of magnesium alloys AZ91 and AZ31. Indication drawn from the study includes that the pressure causes the melting temperatures of the two alloys to increase (AZ91 is 7.58 ° C and 8.70 ° C, respectively, 115 MPa is AZ31), and the total solidification time is significantly reduced.

Furthermore, it has been shown that long freeze range alloys (AZ91) require higher pressures than short freeze range alloys (AZ31) to produce non-porous castings. It was found that a non-porous casting can be obtained under the application pressure of AZ91 of 100 MPa and AZ31 of 50 MPa. Low mold and casting temperatures and high pressures produce fine grain structures in AZ91 and AZ31 castings. The tensile properties of extrusion cast AZ91 and AZ31 are higher than those of gravity casting. Later, another similar survey was conducted during the squeeze casting of the AZ91 [31]. In this study, AZ91 was subjected to squeeze casting under an applied pressure of 138 MPa, a die temperature of 250 ° C and heat treatment under T6 conditions. The results show that compared with the permanent die casting, the squeeze casting significantly improves the tensile properties of the AZ91-T6 alloy, and the microstructure of the extruded AZ91 alloy has fine grains. It has been suggested that in order to lower the porosity of higher castings, a longer pressurization duration is required.

The study by Chadwick et al. [32] finds that the properties of the squeeze cast AZ91 are higher than those cast with other processes such as sand casting, gravity casting and high pressure casting under as-cast and full heat treatment conditions. Figures 2.11 and 2.12 [27] show the changes in the properties of AZ91 produced by different conditions. In all cases, the squeeze cast samples exhibited the highest yield strength, UTS and elongation at break values. The full heat treatment cycle increased the UTS of the squeeze cast sample from 200 MPa to 260 MPa, resulting in a decrease in elongation of only 1%.
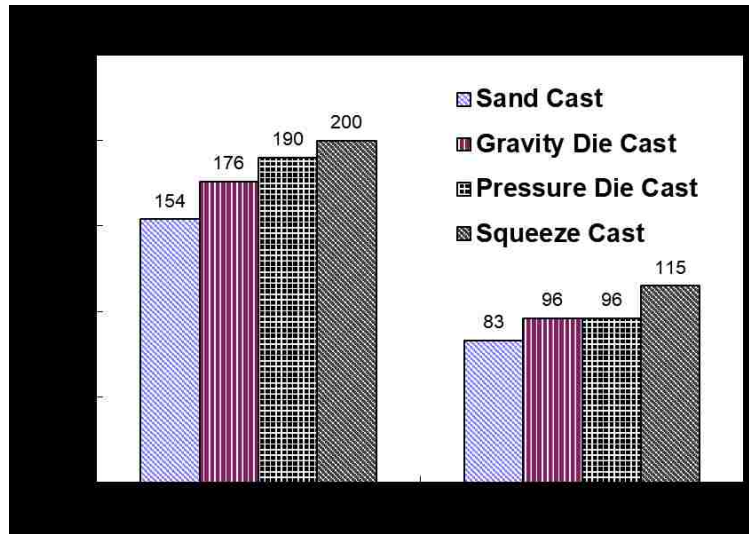
(a)
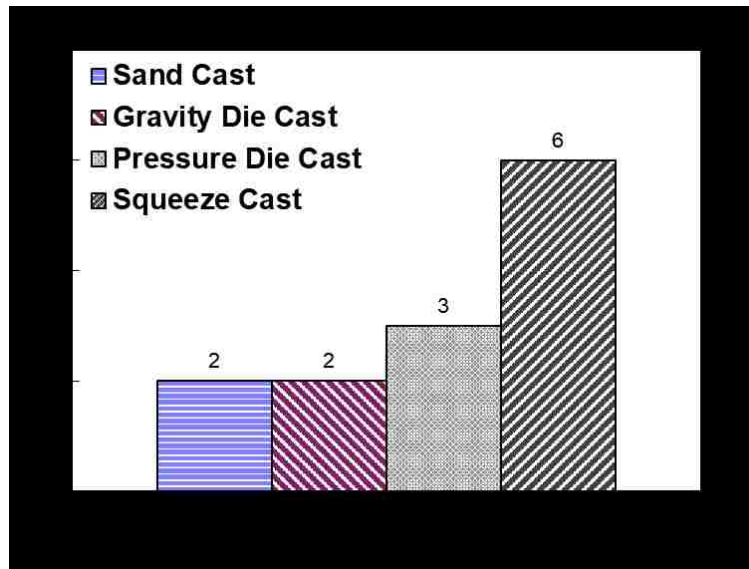
(b)

Figure 2.11 Mechanical properties of cast AZ91 in fully as-cast condition. (a) UTS and yield strength

and (b) elongation [27].
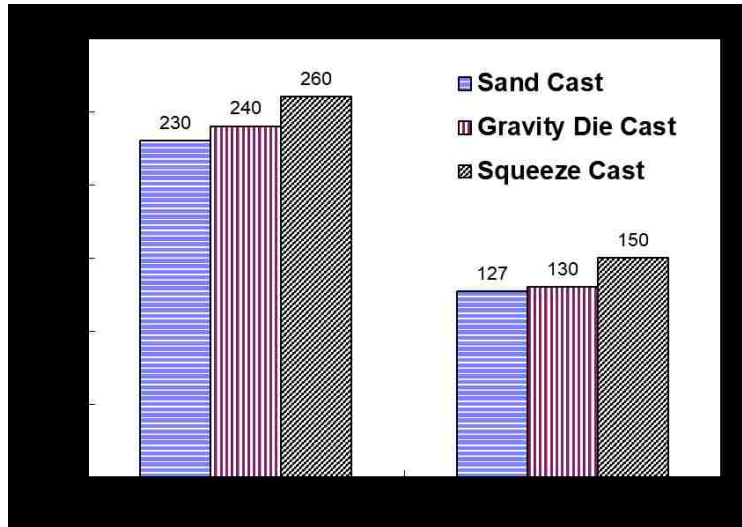
(a)
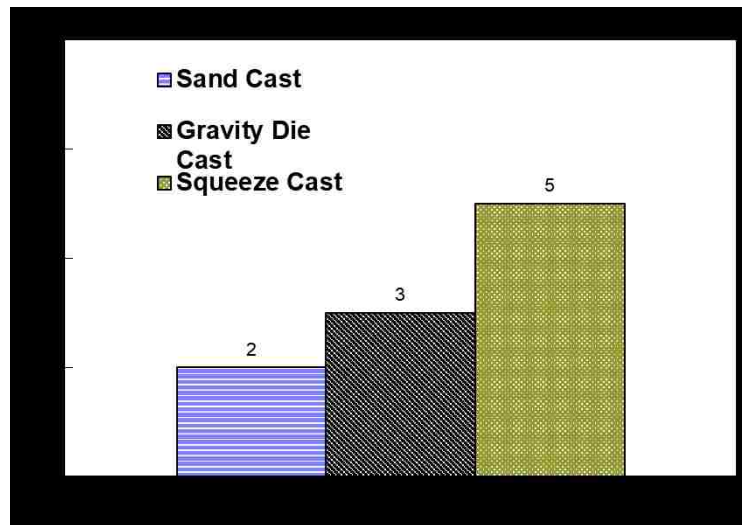
(b)

Figure 2.12 Mechanical properties of cast AZ91 in as-cast condition. (a) UTS and yield strength, (b) elongation [27].

The preliminary study [33] was carried out on the squeeze casting of AZ91D alloy at a pressure of 87 MPa and a die temperature of 450 °C shows that the squeeze cast AZ91D alloy has almost no pores in the microstructure, as shown in Figure 2.13(a). However, as shown in Fig. 2.13(b), typical pores are easily found in high pressure die

cast sheets. Based on the density measurement, the difference in casting stability of the porosity level between squeeze casting and die casting is quantitatively illustrated in Figure 2.14. At this low porosity level, the elongation of the extruded cast sample is expected to be higher. The mechanical properties of the squeeze and die cast alloy AZ91D samples are summarized in Table 2.1.

The elongation of the squeeze cast AZ91D specimens was 5%, 10.5% and 6.5%, respectively, which were 67%, 250% and 117% higher than the as-cast conditions of the as-cast AZ91D. Although the strength (YS and UTS) of the squeeze-cast specimens under as-cast conditions was lower than that of die-casting, the ultimate strength (255 MPa) of the squeeze cst parts after T6 treatment was slightly higher than that of die-cast (230) MPA). The low yield strength and ultimate tensile strength of the squeeze cast specimens under as-cast conditions are directly attributable to their coarse grain and intermetallic compound particles, primarily due to the high mold temperatures used. Higher strengths can be envisaged when further optimizing the parameters of the squeeze casting process. Furthermore, it was confirmed that the parts produced by the squeeze casting were heat treatable compared to the die casting which usually had surface foaming during the heat treatment.

The fracture surface of the tensile specimen was examined by SEM, indicating the difference in fracture behavior between the aqueeze casting and the die casting, as shown in Figure 2.15. It can be clearly seen from Fig. 2.15(a) that the failure of the die cast specimen is caused by the void coalescence as a starting point of the crack and the combined brittle fracture mechanism along the crystal fracture. However, the fracture behavior of the squeeze cast samples is completely different. Their fracture surface is

shown in Figure 2.14(b) and is mainly ductile. The entire fracture surface of the squeeze

cast specimen is characterized by the presence of dimples.

Table 2.1 Tensile Properties of squeeze cast AZ91D Alloy at Room Temperature [33]

Casting Condition		Yield Strength (MPa)	UTS (MPa)	Elongation (%)
Squeeze Cast	as-cast	96	179	5.0
	T4	76	220	10.5
	T6	117	255	6.5
Die Cast (as-cast)		150	230	3.0
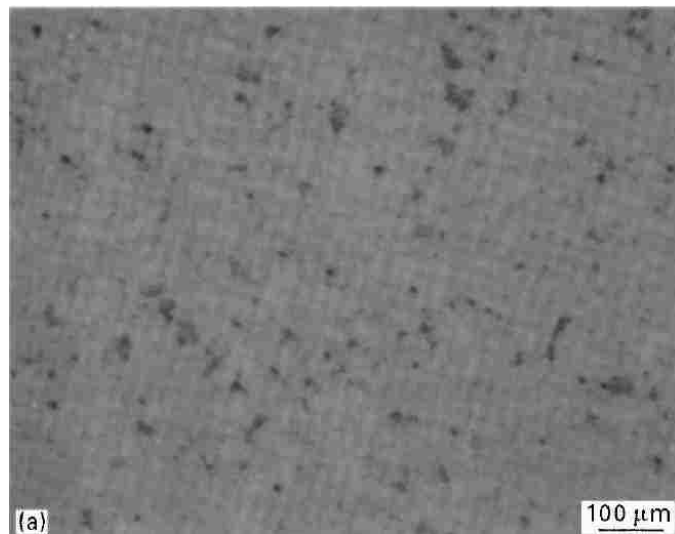
(a)
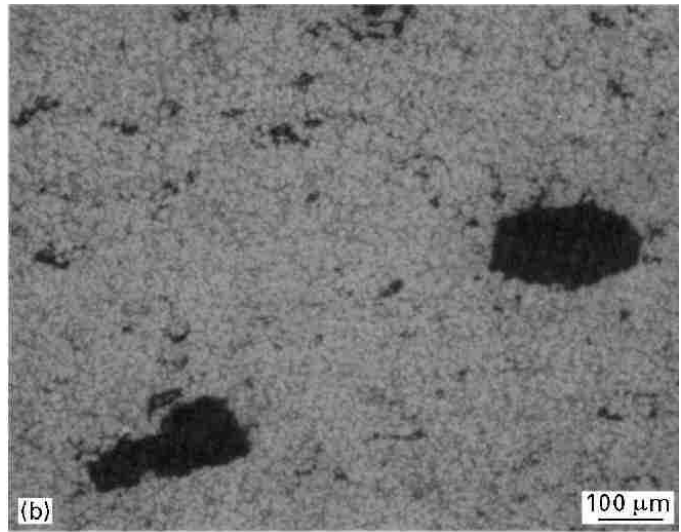
(b)

Figure 2.13 Optical micrographs showing microstructure of (a) a squeeze-cast part,and (b) a die-cast

AZ91D part in the as-cast condition [33].
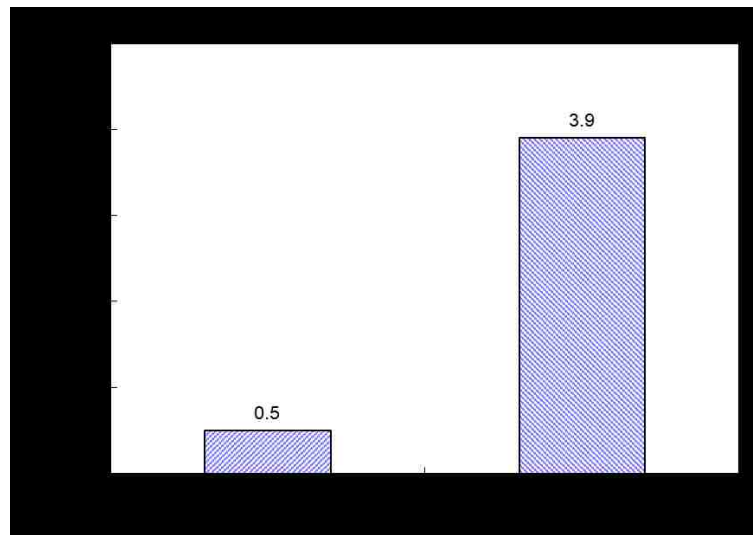
Figure 2.14 Porosity levels of squeeze cast and die cast AZ91D parts with 5 mm section thickness

[33].
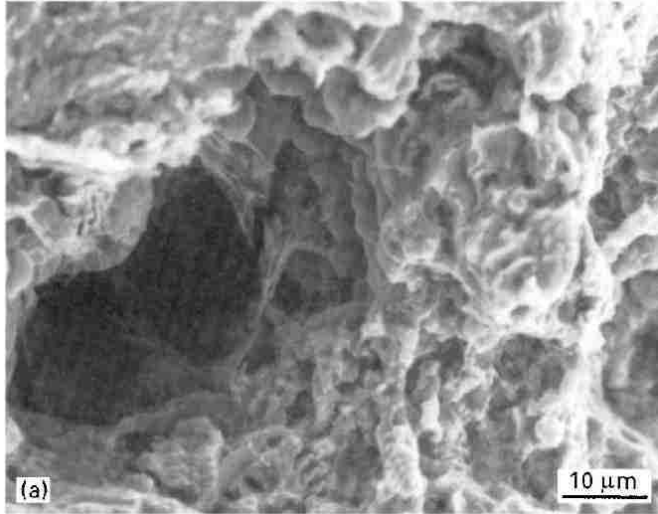
(a)
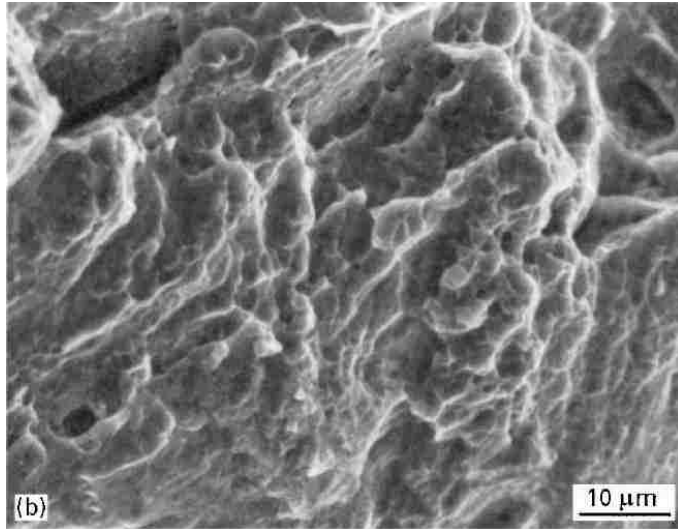
(b)

Figure 2.15 SEM fractographs of AZ91D (a) a die-cast part, and (b) a squeeze-cast part [33].

2.5.1 Galvanic corrosion

When two dissimilar metals are placed in contact in a corrosive or conductive solution, a potential difference produces electron flow between them. The more active metal then becomes anodic and is corroded, and the less active metal becomes cathodic and is protected. This kind of corrosion is called galvanic corrosion, or two-metal corrosion. Magnesium and its alloys are highly susceptible to galvanic corrosion, because magnesium has the lowest standard potential of all the engineering metals as illustrated in Table 2.2 [34].

Table 2.2 Standard EMF series of metals [34]

Galvanic corrosion can also occur between two different phases. Fig. 2.16 illustrated those kinds of galvanic corrosion, external and internal [35]. When magnesium and its alloys are placed contact with other metals, magnesium and magnesium alloys are corroded, while hydrogen gas is evolved on the other metals. When magnesium and magnesium alloys contain second phases because of impurities or alloying elements, the matrix α−phase is corroded, while the hydrogen gas is evolved on the second phases.
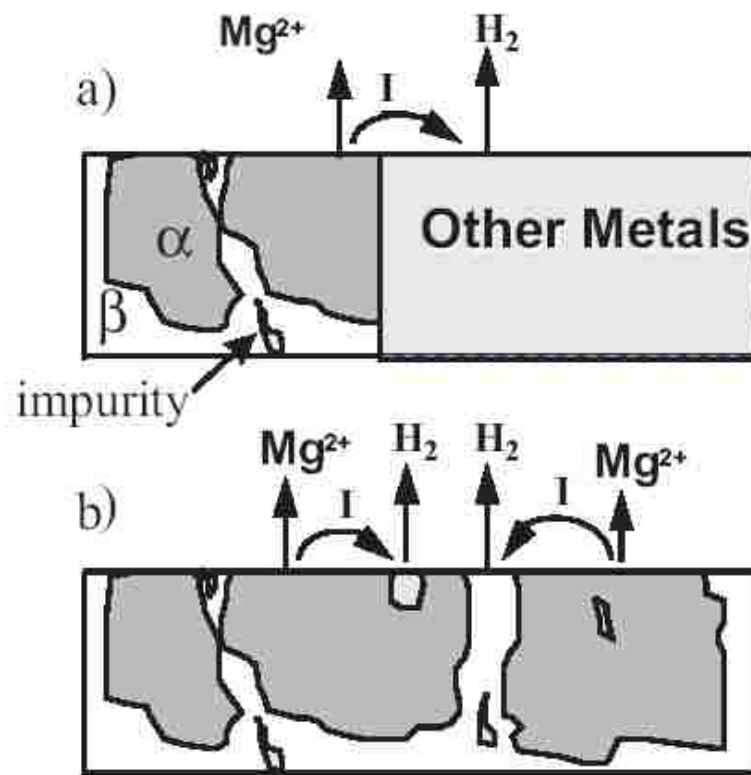
Figure 2.16 a) External galvanic corrosion. b) Internal galvanic corrosion [35].

The galvanic corrosion rate is increased by the following factors: high conductivity of the medium, large potential difference between anode and cathode, large area ratio of cathode to anode, and small distance from anode to cathode [34]. Song et al [36[36]] investigated the corrosion behaviour of AZ91D when it is in contact with aluminum alloy

A380, high strength steel 4150 and pure zinc. It has been found that even though the galvanic effect offers some degree of cathodic protection for aluminum and zinc cathodes, the dissolution of these metals in the salt solution is still unavoidable, particularly in the region far away from the anode/cathode junction. The dissolved Zn^{2+} or Al^{3+} ions flushed to the surface of the AZ91D anode could react to form zinc or aluminum oxides or hydroxides and finally deposit on the AZ91D surface. These products can provide a certain degree of protection for the AZ91D surface.

2.5.2   Stress corrosion cracking (SCC)

Stress-corrosion cracking refers to cracking caused by the simultaneously presence of tensile stress and a specific corrosive medium [34]. Pure magnesium can be considered immune to stress corrosion cracking in both atmospheric and aqueous environments, with no reported failures occurring when loaded to its yield strength [37]. Aluminum containing alloys of magnesium are generally considered the most susceptible to SCC, with the tendency increasing with the aluminum content [37]. The alloys AZ61, AZ80, and AZ91 with 6, 8, and 9% aluminum, respectively, can show high susceptibility to SCC in laboratory and atmospheric exposures, while AZ31, a 3% aluminum alloy used in wrought product applications, is considered to show good corrosion resistance [37]. Magnesium-zinc alloys such as ZK60 and ZE41 that are alloyed with zirconium, or zirconium and rare earth elements, are typically considered only mildly susceptible, while magnesium alloys containing no aluminum or zinc are the most SCC-resistant. For example, M1 alloy, a 1% manganese alloy, like unalloyed magnesium itself, shows no evidence of SCC when placed under tensile stresses as high as its yield strength [35].

SCC in magnesium is mainly transgranular. Sometimes intergranular SCC occurs as a result of $Mg_{17}Al_{12}$ precipitation along grain boundaries in Mg-Al-Zn alloys [35].

2.5.3   Corrosion fatigue

There is very little research on the corrosion fatigue of magnesium alloys. It has been indicated in reference 37 that corrosion fatigue has a close relationship with humidity. For example, AZ31 subjected to an axial load cycle at 10^5 cycles per hour in air and then subjected to increasing levels of humidity showed a slow decrease in the fatigue strength once the humidity exceeded 50%. At 93% relative humidity, the measured fatigue strength had declined to about 75% of that in dry air. It has also been found [35] that corrosion fatigue cracks propagate in a mixed transgranular-intergranular mode and that the corrosion fatigue crack growth rate was accelerated by the same environments that accelerate stress corrosion crack growth. And the corrosion fatigue resistance of AZ91-T6 was significantly reduced in 3.5% salt water relative to that in air.

2.5.4   Pitting corrosion

Few studies have addressed these forms of localized attack of Mg and Mg alloys because other forms of corrosion such as general, galvanic, or stress corrosion are the cause of more serious failure of these materials. The studies of pitting of Mg and Mg are concerned by comparing the pitting behavior of cast to that of rapidly solidified Mg alloys. Makar and Kruger [38] show that rapidly solidified AZ61 exhibits better resistance to pitting than cast AZ61 in a buffered carbonate solution containing various levels of Cl^-. Pit initiation of rapidly solidified AZ61 is found to take place at a higher potential and the pit growth rate is apparently lower than cast AZ61. In the review given by Makar and Kruger [39], it is stated that the difference between the rapidly solidified

and cast Mg. A metallic glass $Mg_{70}Zn_{30}$ exhibits a better resistance to pitting. Also, the film on the metallic glass is more protective against pitting attack than the pure Mg. The glassy Mg alloy is found to exhibit a more stable passive film than pure Mg, Zn or several other crystalline Mg-based alloys. Heavy metal contamination promotes general pitting attack. In Mg-Al alloys, pits are often formed due to selective attack along $Mg_{17}Al_{12}$ network that is followed by the undercutting and falling out of grains [35].

2.6.1   Introduction of Plasma Electrolytic Oxidation coating

Plasma Electrolytic oxidation (PEO), also called plasma anodizing or micro arcing, is a promising surface treatment for hexavalent chromium replacement in anti-corrosion protection or in the improvement of the tribological properties of lightweight metal structures. This electrolytic plasma oxidation can be distinguished from classical anodizing by the use of voltages above the dielectric breakdown potential of the anodic oxide being formed. This leads to the local formation of plasmas, as indicated by the presence of sparks that are accompanied by a release of gas [40].

The PEO coatings exhibited better corrosion resistance than the coatings treated by anodizing. Zhang et al [41] compares the oxide coatings produced by the PEO process with the anodic coatings prepared by the HAE and Dow 17 process. It has been found that the PEO coatings are smooth, uniform, in contrast to rough, patchy film produced by HAE and relatively rough, even, partly powdery film produced by DOW17. Furthermore, the films produced by the EPO process are much more corrosion protective than those produced by HAE and DOW17.

2.6.2 The PEO Coating Process

The PEO process involves anode electrochemical dissolution, the combination of metal ions with anions to form ceramic compounds and sintering on the substrate under the action of the sparks. Plasma electrolytic oxidation (PEO) technology has been used for depositing ceramic coatings on magnesium alloys for corrosion protection [41-44]. The coatings can be as thick as a few hundreds of micrometers and their corrosion behavior strongly depends on the process parameters employed, the chemical compositions of the materials studied, and the electrolytes used. The effect of electrolyte composition on properties of PEO oxide coatings on Mg and Mg alloys has also been an interesting subject of investigation to the automobile industry. The electrolytes consisted of potassium hydroxide and some other passive agents can modify the characteristics of the oxide coatings. Hsiao and Tsai [43] studied the characteristics of anodic films formed on solutions containing 3M KOH, 0.21M $NaPO_4$, 0.6 MKF, with and without $Al(NO_3)_3$. The addition of Al $(NO_3)_3$ into 3 M KOH+0.21 M Na_3PO_4 +0.6 M KF base electrolyte assists uniform sparking on AZ91D magnesium alloy in anodizing. Either with or without a low concentration of Al $(NO_3)_3$, a porous and non-uniform anodic film is formed. The presence of Al $(NO_3)_3$ in the base electrolyte results in the formation of Al_2O_3 and $Al(OH)_3$ in the anodic film. The presence of Al_2O_3 in the films is beneficial to the corrosion resistance of films in 3.5 wt% NaCl solution.

The process parameters employed also play an important role in the characteristics of oxide coatings. Zhang et al. [41] indicate that the properties of oxide coatings are strongly influenced by the process parameters employed. With an increase in solution temperature, the film thickness decreases. On the other hand, the film thickness increases with an

increase in treatment time and current density. The voltages rise during the PEO process is always accompanied by the increase of film thickness. Higher voltage produces thicker film. Khaselev et al [42] investigats the characteristics of the oxide coatings on binary Mg-Al alloys in a solution containing 3 M KOH, 0.6 M KF, and 0.21 M Na_3PO_4 with 1.1 M aluminate. The breakdown voltages increases with an increase in Al content in the alloys. The growth of oxide films is non-uniform. The growth starts on α-Mg and continues on the β-phase ($Mg_{17}Al_{12}$) when the voltage exceeds 80 V, and a uniform anodic film is formed on the alloy substrate when the voltages reached 120 V. Al is incorporated into oxide coatings from both the substrate and the electrolyte.

From the literature review, it can be concluded that, despite of the availability of data of section thickness-dependent mechanical properties, detailed information on the relationship between section thicknesses, microstructure and tensile behavior and porosity level is limited for high pressure die cast (HPDC) magnesium alloy AZ91. Literatures on the microstructure and mechanical properties of high pressure die cast magnesium alloy are limited comparing to those aluminum alloys. A systematic research in understanding the microstructure and mechanical properties of high pressure die cast magnesium alloy AZ91 is needed for further expanding magnesium applications in automobiles.

Plasma electrolytic oxidation is the most widely commercially used coating technology for magnesium and its alloys. This process is technologically more complex than other coating methods but is less sensitive to the type of alloys being coated. Although the process is relatively expensive due to the need for cooling systems and

high-power consumption, this expense could be evened out by its low waste disposal, high effectiveness and environmental friendliness. The PEO coatings produced by anodizing are porous ceramic-like films. These properties impart good paint-adhesion characteristics and excellent wear and abrasion resistance to the coating. Studies have proofed and developed appropriate coating schemes for the protection of magnesium for use in corrosion resistant. PEO Coating technology has been developed, which functions to adequately protect magnesium from corrosion in harsh service conditions. Overall it appears that the PEO coating is increasingly becoming the leading technology for magnesium alloys to improve corrosion resistance, especially since the process is environmentally friendly and capable of providing thick and hard ceramic coating.

It is evident that there is little information comparing the effect of the section thicknesses and the effect of PEO coating on mechanical properties of high pressure die cast AZ91 alloy. Hence, this study includes two parts. Part one is to investigate how the section thickness of HPDC magnesium alloy AZ91 affect the mechanical properties; and part two is to evaluate the PEO coating effect on mechanical properties of HPDC Mg alloy AZ91 with through three different section thickness.

[1] G. V. Raynor., "The Physical Metallurgy of Magnesium and its Alloys", Pergamon Press, 1959.

[2] E. F .Emley, "Principles of Magnesium Technology", Pergamon Press, 1966.

[3] L. Y.Wei., "Development of Microstructure in Cast Magnesium Alloys", PH.D. Thesis. Chalmers University of Technology, Goteburg, Sweden, 1990.

[4] L. F. Mondolfo., "Maganese in Aluminium Alloys", The Manganese Centre, France, 1978.

[5] F. A .Fox.: J. Inst. Metals, Vol 71, p415-439, 1945.

[6] J.L. Murray., Binary Alloy Phase Diagrams, ed. Massalski. T. B, ASM, Ohio, pg. 169-171, 1991.

[7] M. Hansen.: "Constitution of Binary Alloys", McGraw Hill Book Company, 1958.

[8] Winston Sequeira, " The Microstructure and Mechanical Properties of High Pressure Diecast Magnesium Alloy AZ91D", PHD thesis, University of Queensland, Brisbane, Australia, pp.17, 2000.

[9] M.C. Flemings.: Solidification Processing, McGraw Hill Inc., 1974

[10] H. Iimi, Y. Kameyama, Y. Naganawa, E. Kato, H. Nomura, "More Accurate Die Casting Fluid Fow Simulation by Direct Observation of Die Cavity Filling" NADCA Transactions, Indianapolis, T03-016, 2003

[11] Internet article: Introduction to High Integrity Die Castin Process, Http: www.media.wiley.com/product_data/excerpt/16/04712013/0471201316.pdf.

[12] Internet article, Die Casting Process Basic, Http: www.diecasting.org/faq/.

[13] A. Gordon., G. Meszaros, J. Naizer, C. Mobley, "Equations for Predicting the Percent Porosity in Die Castings", paper No T93-024, Trans NADCA International Die Casting Congress and Exposition, Cleveland, 1993

[14] H. Gjestland, S. Sannes, H. Westengen, D. Albright, "Effect of Casting Temperature, Section Thickness and Die Filling Sequence on Microstructure and Mechanical Properties of High Pressure Die Castings" NADCA Transactions, Indianapolis, T03-036, 2003.

[15] H. Mao, J. Brevick, C. Mobley and V. Chandrasekar, "Effects of Section Size and Microstructural Features on the Mechanical Properties of Die Cast AZ91D and AM60B Magnesium Alloy Test Bars", SAE Technical Paper Series, 1999-01-0927.

[16] R.M. Wang, A. Eliezer, E.M. Gutman, "An investigation on the Microstructure of an AM50 Magnesium Alloy", Material Science and Engineering A335(2003) 201-207.

[17] G. Chadha, J. E. Allison, J. W. Jones, "The role of Microstructure and Porosity In Ductility of Die Cast AM50 and AM60 Magnesium Alloys.

[18] M. C. Flemings, R. W. Strachan, E. J. Poirier, and H. F. Taylor, "Performance of Chills on High Strength Magnesium Alloy Sand Castings of Various Section Thickness", Transaction of the American Foundrymen's Society, Vol. 66, pp. 336-343, 1958.

[19] I. J. Feinberg, and J. D. Grinsley, "Tensile Properties of Microshringage-graded AZ-63 Magnesium Alloy", Transaction of the American Foundrymen's Society, Vol. 66, pp. 409-414, 1958.

[20] G. W. Form, P. J. Ahearn, and J. F. Wallance, "Mass Effect on Castings Tensile Properties", Transaction of the American Foundrymen's Society, Vol. 67, pp. 64-69, 1959.

[21] R. D. Green, "Porosity-Free Magnesium Alloy Castings Thermal Requirements", Transaction of the American Foundrymen's Society, Vol. 68, pp. 245-252, 1960.

[22] A. Couture and J.W. Meier, "The Effect of Wall Thickness on Tensile Properties of Mg-Al-Zn Alloy Castings", Transaction of the American Foundrymen's Society, Vol. 74, 164-173, 1966.

[23] W. P. Sequeira, M. T. Murra, G. L. Dunlop and D. H. St. John, "Effect of Section Thickness and Gate Velocity on the Microstructure and Mechanical Properties of High Pressure Die Cast Magnesium Alloy AZ91D", Automotive Alloys, Edited by DAS, TMS, 168-180, 1997.

[24] M. Murray, W. P Sequeira, and R. D'Allesandro, "Properties and Design of Castings in Magnesium Alloy AZ91D", SAE Technical Paper Series, Paper 960420, 41-47, 1996.

[25] G. Schindelbacher and R. Rosch, "Mechanical Properties of Magnesium Die Casting Alloys at Elevated Temperatures and Microstructure in Dependence of Wall Thickness', Austrian Foundry Society Wolfsberg Conference, 247-252, 1998.

[26] W.P. Sequeira, M.T. Murray, G.L. Dunlop, D.H. St. John, "Effect of Section Thickness and Gate Velocity on the Microstructure and Mechanical Properties of High Pressure Die Cast Magnesium Alloy AZ91D, in: S.K. Das(Ed.) Automotive Alloys, TMS, Warrendale, PA, pg. 169-183, 1997.

[27] H. Hu, Squeeze Casting of Magnesium Alloys and Their Composites, Journal of Materials Science Vol. 33, 1579-1589, 1998.

[28] M.R. Ghomashchi, A. Vikhrov " Squeeze casting: an overview", Journal of Materials Processing Technology 101 (2000) 1-9.

[29] S. Li, S. Sanakanishi, M. Tsunoi, M. Akase, K. Anzai, "Method for Numerical Prediction of Porosity in Squeeze Casting", NADCA Transactions, Indianapolis, 2003, T03-014.

[30] H.U. Ha, "Squeeze Casting of Magnesium-Based Alloys and Their Metal Matrix Composites", Ph.D thesis, Department of Engineering Materials, University of Southampton, 1988.

[31] G.A. Chadwick and A. Bloyce, "Squeeze Cast Magnesium Alloys and Magnesium Based Composites", Proc. Conf. Magnesium Alloys and Their Applications, Garmisch-Partenkirchen, Germany, Apr. 1992, 93-100.

[32] G.A. Chadwick and T.M. Yue, "Principles and Applications of Squeeze Casting", Metals and Materials, 5, No.1, 1989, 6-12.

[33] A. Luo, H. Hu and S.H.J. Lo, "Microstructure and Mechanical Properties of Squeeze Cast AZ91D Magnesium Alloy," Light Metals Symposium, CIM, Montreal, 1996.

[34] M. G. Fontana, "Corrosion Engineering", 3rd Ed., McGraw-Hill International Editions, USA, 1996.

[35] G. Song and A. Atrens, "Corrosion Mechanisms of Magnesium Alloys", Advanced Engineering Materials, 1 (1999) 11-33.

[36] G. Song and B. Johannesson, S. Hapugoda and D. StJohn, "Galvanic corrosion of magnesium alloy AZ91D in contact with an aluminium alloy, steel and zinc", Corrosion Science, 46 (2004) 955-977.

[37] R. Baboian, S. Dean, H. Hack, G. Haynes, J. Scully, D. Sprowls, "Corrosion Tests and Standards: Application and Interpretation", ASTM Manual Series: MNL 20, Philadelphia, USA, 1995.

[38] G. L. Makar and J. Kruger, "Corrosion studies of rapidly solidified magnesium alloys", Journal of the Electrochemical Society, 137 (1990) 414-421.

[39] G. L. Makar and J. Kruger, "Corrosion of magnesium", International Materials Reviews, 38 (1993) 138-153.

[40] A. L. Yerokhin, X. Nie, A. Leyland, A. Matthews and S. J. Dowey "Plasma electrolysis for surface engineering", Surface and Coatings Technology, 122 (1999) 73-93.

[41] Y. Zhang, C. Yan, F. Wang, H. Lou and C. Cao, "Study on the environmentally friendly anodizing of AZ91D magnesium alloy", Surface and Coatings Technology, 161 (2002) 36-43.

Magnesium alloys, as one of the attractive lightweight materials, are utilized widely in the automotive industry due to market demand for high gas mileages of vehicles and government regulations for low greenhouse gas emission. Presently, conventional high pressure die casting (HPDC) process are primarily employed by the automotive industry for production of magnesium alloy-based lightweight components such as radiator support, instrumental panels and steering column support brackets [1-4]. HPDC Mg components usually have various wall stocks around 5 mm and moderate mechanical properties. It is crucial to understand the relationship between the mechanical properties including ultimate tensile strength (UTS), 0.2% yield strength (YS) and elongation (e_f) and the wall stocks of HPDC magnesium alloys for the purpose of engineering design [5, 6]. Previous studies were focused on the HPDC Mg alloys with relatively thin wall stocks since the nominal thickness of most current thin-wall Mg components is around 5 mm, although the effect of wall stocks on their mechanical properties was investigated [7, 8]. In this research, the influence of wall thicknesses on microstructure evolution and mechanical properties of relatively thick HPDC AZ91 alloys (10 mm and 6 mm) was studied in comparison with the thin wall (2 mm) counterpart. Microstructural analyses and mechanical testing on the HPDC AZ91 alloy were performed. The effort of establishing the relation between the thin and thick wall stocks up to a thickness of 10 mm, microstructure and mechanical properties of the HPDC were made.

3.2.1   Material and Process

The commercially available magnesium alloy AZ91 (Mg-8.48wt.%Al-0.61wt.%Zn-0.18wt.%Mn) was used. A 700-ton cold chamber horizontal high pressure die casting machine was employed for producing specimens which had a rectangular shape of 125 mm by 27 mm and a desired wall thicknesses of 2 mm, 6 mm or 10 mm.

3.2.2   Porosity Measurement

Porosity contents of specimens were measured based on Archimedes principle. After specimen weights were measured in air and distilled water, Equation 3.1 was used to calculate the actual density (ρ_a) of each specimen according to ASTM Standard D3800:

$$\boldsymbol{\rho_a} = \frac{W_a \times \rho_w}{W_a - W_w} \qquad \text{Equation 3.1}$$

where W_a equals to the weight in air and W_w equals to the weight in water, and ρ_w equals to the density of water. Equation 3.2 was applied for computing the porosity content (P %) according to ASTM Standard C948:

$$\boldsymbol{P}\% = \boldsymbol{100}\% \times \frac{\rho_t - \rho_a}{\rho_t} \qquad \text{Equation 3.2}$$

where ρ_t is the theoretical density of the alloy AZ91, with density 1.81 g/cm^3 [5].

3.2.3   Microstructure

Metallographic samples were cut from the center of cast specimens. The standard mounting and polishing procedure were applied to the cut metallographic samples subsequently before the observation. An etchant of 60% ethanal-20% acetic acid-19% distilled water-1% nitric acid was applied to the polished specimens for microscopic

examination. An optical microscope was employed to characterize primary features of the prepared sample. The detailed features of the microstructure were also characterized at high magnifications by a scanning electron microscope (SEM), Hitachi Tabletop Microscope TM3000, with a maximum resolution of 30 nm in a backscattered mode/1 μm in x-ray diffraction mapping mode, and useful magnification of 15–30,000.

3.2.4   Tensile Testing

An Instron machine integrated with a digital data recording system was used to determine the tensile properties of the HPDC AZ91 alloy with various wall stocks at room temperature. Based on ASTM B557, tensile samples with a gage length of 25 mm, a width of 6 mm, and a wall thickness of 2 mm, 6 mm, or 10 mm were prepared from HPDC specimens. According to the averaged results of three tests, yield strength (YS), ultimate tensile strength (UTS), and elongation to failure (e_f) of the HPDC AZ91 alloy were determined.

3.3.1   Porosity Content

Figure 3.1 presents the SEM micrographs, showing the porosity contents in the HPDC AZ91 alloy. Despite the presence of very few and small pores in the 2 mm specimens as shown in Figure 3.1 (a), a large number and sizes of pores are easily observed in the 6 mm and particularly in the 10 mm specimens as illustrated in Figure 3.1(b) and Figure 3.1(c).
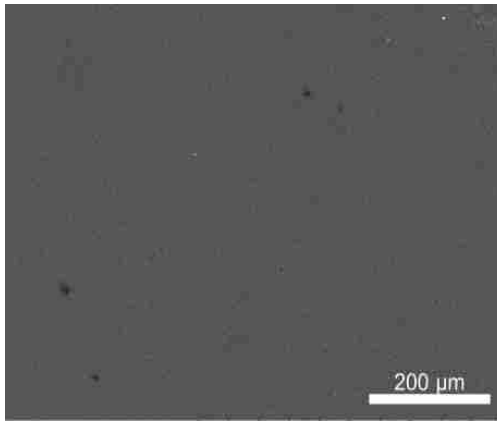
(a)
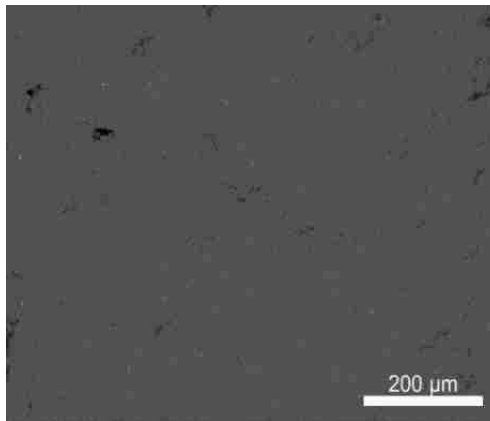
(b)
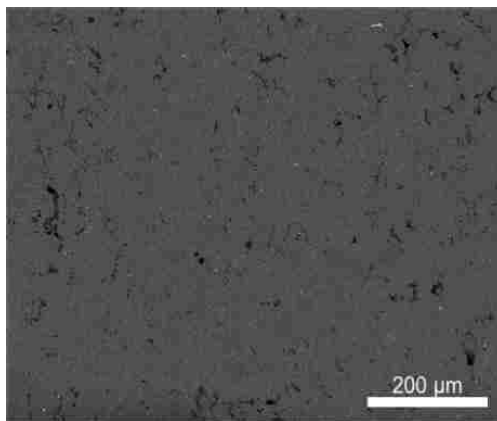
(c)

Figure 3.1 SEM microstructure of die cast AZ91 alloy with wall thicknesses (a) 2, (b) 6, and (c) 10

mm.

The measured porosity contents of the HPDC AZ91 alloy specimens with the wall stocks of 2 mm, 6 mm and 10 mm are presented in Figure 3.2. It can be seen that the 6 mm and 10 mm specimens have the high porosity contents of 2.61% and 3.57%, respectively, while there is a very low porosity content of only 0.53% in the 2 mm one. Examination of the measured porosity contents manifests the differences in casting quality resulting from variation in wall stocks. As the wall thickness increases, the porosity content of the HPDC AZ91 alloy increases and its entrapped pores become large.

The very fast filling of high temperature melts into mold and the high cooling rates lead to the very low porosity content of the 2 mm specimen. The implication from computer simulation of mold filling and heat transfer of the HPDC AZ91 alloy indicates that the existence of high porosity contents in the thick 6 mm and 10 mm specimens might be attributed to poor filling and slow solidification [9].
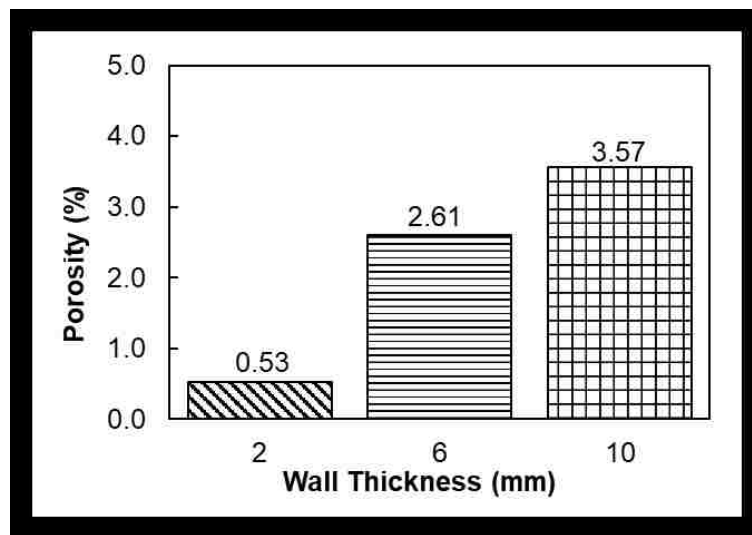
Figure 3.2 Porosity content vs. wall thicknesses

3.3.2   Microstructure

Figure 3.3 gives optical micrographs showing the existence of a fine microstructure in the outer skins of the HPDC AZ91 alloy for the 2 mm and 10 mm specimens. The

observation on the presence of large primary α-Mg dendrites in the 10 mm specimen reveals the distinct difference in the microstructure of the skin from the 2 mm specimen. In the center region of the 10 mm HPDC AZ91 alloy specimen, there are also large primary α-Mg dendrites as shown in Figure 3.4. In contrast, the dendrites in the 2 mm specimen are much smaller.

(a)   (b)
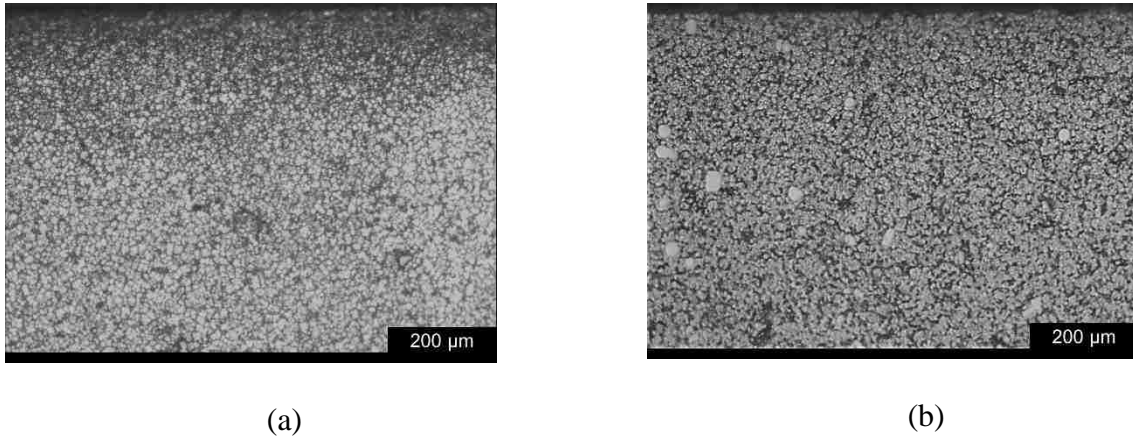
Figure 3.3 Optical micrograph showing microstructure in the skin of the HPDC AZ91 alloy with difference wall thicknesses, (a) 2 mm and (b)10 mm.

To understand the development of the observed microstructure of the HPDC AZ91, the filling and solidification sequences of the conventional HPDC process need to be taken into consideration. The process starts with pouring the liquid metal at a desired temperature into a shot sleeve. The direct contact between the liquid metal and the sleeve chills the metal rapidly to its liquidus temperature and kicks off solidification. The formation of a high-volume fraction of the primary α-Mg dendrite occurs in the sleeve prior to the metal arrives at the gate of the cavity. Once the partially-solidified metal is pushed into the cavity, the pre-formed α-Mg crystals float in the melt, which are present in the finally-solidified HPDC microstructure [5, 10]. Due to the fast cooling at the interface between the casting and die, the surfaces of the specimens become the location

to form fine grains. In the center of the specimens, the solidification for the 6 and 10 mm thick specimen due to their thick walls takes place much more slowly than that of the 2 mm one. As a result, the coarse microstructure develops in the 10 mm thick specimen compared to that formed in the 2 mm one.

(a)   (b)
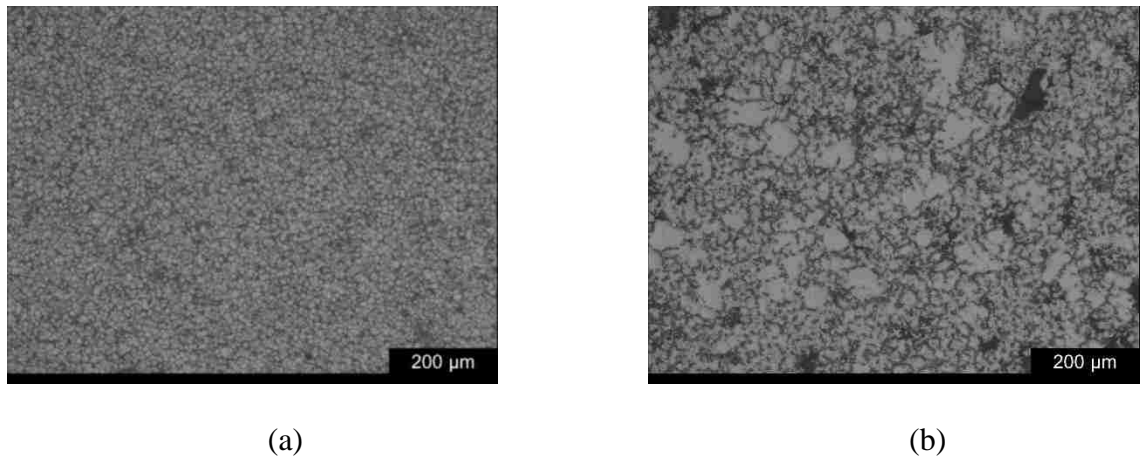
Figure 3.4 Optical micrographs showing microstructure in the center of the HPDC AZ91 alloy with difference wall thicknesses, (a) 2 mm and (b) 10 mm

3.3.3   Tensile Properties

Typical tensile engineering stress vs strain curves of the HPDC AZ91 alloy with the 2 mm, 6 mm and 10 mm thicknesses are given in Figure 3.5. For all the three wall stocks, the stress changes with the strain in the similar trends. Upon the application of tensile loads, the elastic deformation of the alloy commences. With increasing the load, the alloy arrives at its yield point. Then, the alloy deforms plastically. As the load further increases and reaches its UTS, the fracture of the alloy occurs. Both the plastic deformations and fracture for the 10 mm thick specimen take place at much lower stress and strain levels than those of the 2 mm and the 6 mm ones.
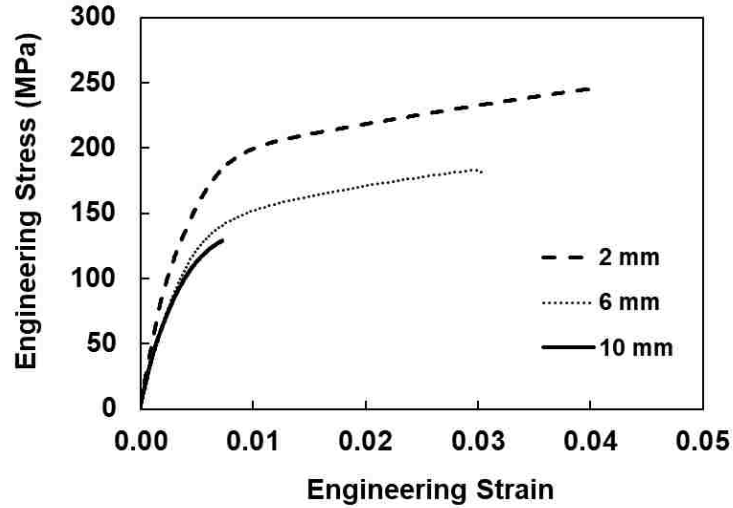
Figure 3.5 Typical tensile engineering stress vs strain curves of the HPDC AZ91 alloy.

Table 3.1 lists the UTS, YS and e_f for all the three wall stocks. It can be seen that the UTS and YS increases to 245.5 and 169.3 MPa for the 2 mm thick specimens from 129.2 and 110.6 MPa for the 10 mm coupons, which exhibits over 90% and 53% increases in UTS and YS, respectively. Also, a large increase in elongation appears when the wall thickness of the specimens decreases, since the elongation values, 4.1%, 3.0% and 0.7% for the 2 mm, 6 mm, and 10 mm respectively. The results of the current study are consistent with the relationship between tensile properties and wall thicknesses for different types of the die casting magnesium alloys reported in the literature [6, 7]. The changes in strengths and elongation should be attributed to the differences in the porosity content and the microstructure characteristics of the HPDC AZ91 alloy. The increases in the tensile properties results from the fine microstructure and low porosity content of the thin specimen. On the contrary, the coarse microstructure, the high porosity contents and the presence of large pores reduce strengths and elongations of the thick specimens.

48

Table 3.1 Tensile properties of the HPDC AZ91 alloy

Wall Stock (mm)	UTS (MPa)	0.2% YS (MPa)	Elongation (%)
2	245.5 ±5.7	169.3 ± 5.5	4.1 ±0.34
6	182.9 ±4.8	132.0 ±4.0	3.0 ±0.18
10	129.2 ±7.11	110.6 ±6.8	0.7 ±0.21

The microstructural characteristics of the HPDC AZ91 alloy with three different wall stocks, 2 mm, 6 mm and 10 mm are investigated. The wall thickness affects microstructure development of the HPDC AZ91 alloy. The relatively thick wall stocks leads to the formation of large pores and large primary α-Mg dendrites, and high porosity contents in the HPDC AZ91.

The tensile properties, UTS, YS, and e_f, are considerably reduced by the thick wall stocks. The UTS and YS decreases to 129.2 and 110.6 MPa for the 10 mm thick specimen from 245.5 and 169.3 MPa for the 2 mm one, which exhibits over 47% and 35% decrease in UTS and YS, respectively. Also, a large decrease of 82% in elongation appears when the wall thickness of the specimens increases from the 2 mm to 10 mm, since the elongation values, 4.1%, and 0.7% for the 2 mm and the 10 mm respectively. Overall, it appears that the conventional HPDC is capable of producing the sound AZ91 casting, with a thickness up to 6 mm, and fails to manufacture the AZ91D alloy with thick wall stock of 10 mm, which has insufficient tensile properties.

[1] K. Guan, B. Li, Q. Yang, X. Qiu, Z. Tian, D. Zhang, D. Zhang, X. Niu, W. Sun, X. Liu and J. Meng. "Effects of 1.5wt% samarium(Sm) addition on microstructures and tensile properties of a Mg-6.0Zn-0.5Zr alloy," J. Alloys and Compounds Vol. 735, pp. 1737, 2018.

[2] Y.Y Li, W.M. Zhao, J. Ding and H.T. Xue, "Ignition-proof performance and mechanism of AZ91D-3Nd-xDy magnesium alloys at high temperatures" China Foundry Vol.15 No.2 (2018), pp. 97, 2018.

[3] B.R. Powell, V. Rezhets, M.P. Balogh and R.A.Waldo, "Microstructure and creep behavior in AE42 magnesium die-casting alloy" JOM,Vol 54, pp. 34, August 2002.

[4] A.A. Luo, "Magnesium casting technology for structural application,"Journal of Magnesium and Alloys Vol. 1, issue 1, pp. 2, March 2013.

[5] M.M. Avedesian, and H. Baker, *Magnesium and Magnesium Alloys-ASM Specialty Handbook* ,ASM Int., Materials Park, OH, USA, 1999.

[6] M. Zhou, N. Li and H. Hu, "Effect of Section Thicknesses on Tensile Behavior and Microstructureof High Pressure Die Cast Magnesium Alloy AM50," Material Science Forum Vols. 475-479 , pp. 463, 2005.

[7] C.H. Cáceres, W.J. Poole, A.L. Bowles and C.J. Davidson, "Section thickness, microhardness and yield strength in high -pressure diecast magnesium alloy AZ91" Materials Science and Engineering A,Vol. 402 *Issues* (1-2) , pp. 269, August 2005.

[8] S.L. Sin, D. Dubé and R. Tremblay, "An investigation on microstructural and mechanical properties of solid mould investment casting of AZ91D magnesium alloy," Materials Characterization Vol. 59, Issues (2) , pp.178, February 2008

[9] H. Hu and Z. Sun: Internal Research, University of Windsor, 2018.

[10] R.M. Wang, A. Eliezer and E.M. Gutman, "An investigation on the microstructure of an AM50 magnesium alloy," Material Science and Engineering A Vol. 355, Issues 1-2, , p.g 201, 2003.

██ ████████████

Magnesium usage in automobiles has arisen significantly due to consumer demands for increased performance and fuel economy of vehicles. Most magnesium applications presently used in the automotive industry are high-pressure die cast (HPDC) and have relatively good strengths and high ductility at room temperature. Applications of HPDC magnesium alloys, such as front-end support assemblies, steering wheel armatures and steering column support brackets [1, 2], have not only complex shapes but also cross sections with various thicknesses. Very often, under normal die casting conditions, thick sections have a higher tendency to solidification shrinkage and porosity caused by inclusion of gas than thin walls. It has been indicated [3-6] that the porosity level of HPDC Mg alloys influences mechanical properties, such as ultimate tensile strength (UTS), 0.2% yield strength (YS) and elongation (e_f). Cáceres et al [7] attempted to establish the relationship between the hardness and yield strength for the HPDC AZ91 with the section thickness upto 5 mm, while the study by Sin et al [8] showed the tensile properties of the plaster mold cast AZ91 with the section thicknesses of 1 to 4.3 mm, which were compared with those of the HPDC counterpart. Gjestland et al [9] present the tensile properties of the HPDC AZ91 alloy with the section thicknesses varying from 1 to 9 mm, but failed to provide detailed analyses of plastic deformation, and tensile and fracture behaviors.

This paper presents an in-depth analysis of strain-hardening behaviour during plastic deformation and fracture characteristics of the HPDC AZ91 alloy with section

thicknesses of 2, 6 and 10 mm. The influence of section thicknesses on plastic deformation behaviour of the alloy was studied based on the analysis of true stress-strain relation. The fracture behaviour of the HPDC AZ91 affected by section thicknesses was characterized by using SEM fractography.

■ ▬▬▬▬▬▬▬▬▬▬

4.2.1 Alloy and Casting Preparation

The magnesium alloy selected in this study was die casting Mg-8.48 wt.%Al-0.61 wt.%Zn-0.18 wt.%Mn alloy AZ91D. Flat rectangular coupons of 125 mm × 27 mm with different section thicknesses of 2, 6 and 10 mm were die cast on a 700 ton cold chamber horizontal high pressure die casting machine.

4.2.2 Porosity Measurement

Porosity contents of specimens was measured based on Archimedes principle. After specimen weights were measured in air and distilled water, Equation 4.1 was used to calculated the actual density (ρ_a) of each specimen according to ASTM Standard D3800:

$$\boldsymbol{\rho_a} = \frac{W_a \times \rho_w}{W_a - W_w} \qquad \text{Equation 4.1}$$

where W_a equals to weight in air and W_w equals to weights in water, and ρ_w equals to density of water. Equation 4.2 was applied for computing the porosity percentage (P%) according to ASTM Standard C948:

$$\boldsymbol{P\%} = \boldsymbol{100\%} \times \frac{\rho_t - \rho_a}{\rho_t} \qquad \text{Equation 4.2}$$

where ρ_t is the theoretical density of the alloy AZ91, i.e., 1810 kg/cm^3 [5].

4.2.3   Tensile Testing

The mechanical properties of the HPDC AZ91 alloy with various thickness were evaluated by tensile tests, which were performed at ambient temperature on an Instron machine equipped with a computer data acquisition system. Following ASTM B557, subsize flat tensile specimens (25 mm in gage length, 6 mm in width, and 2, 6, 10 mm in as-cast thicknesses) were machined from the die cast coupons. The tensile properties, including 0.2% yield strength (YS), ultimate tensile strength (UTS), and elongation at fracture (e_f), were obtained based on the average of three tests.

4.2.4   Characterization of Microstructure and Fractured Surface

Specimens were sectioned, mounted, and polished from the center of the coupons and prepared following the standard metallographic procedures. An etchant of 60% ethanal-20% acetic acid-19% distilled water-1% nitric acid was applied to polished specimens for microscopic examination. A Buehler optical image analyzer 2002 system was used to determine primary characteristics of the specimens. The detailed features of the microstructure were also characterized at high magnifications by a scanning electron microscope (SEM), Hitachi Tabletop Microscope TM3000, with a maximum resolution of 30 nm in a backscattered mode (BSE)/1 μm in x-ray diffraction mapping mode, and useful magnification of 10–30,000.

4.3.1   Porosity Content

Figure 4.1 presents the SEM micrographs, showing the porosity contents in the HPDC AZ91 alloy. Despite the presence of very few and small pores in the 2 mm specimens as shown in Figure 4.1(a), a large number of big pores are easily observed in both the 6 and 10 mm specimens as illustrated in Figure 4.1(b) and (c).
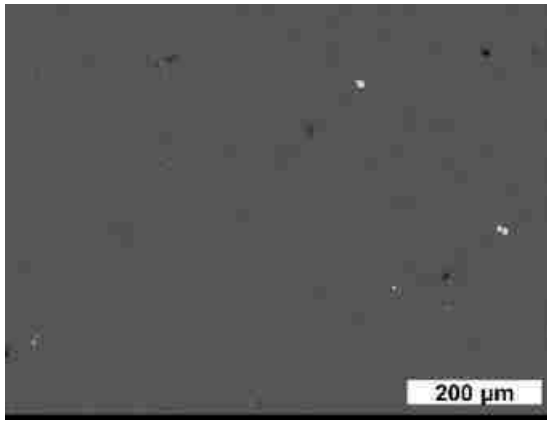
(a)
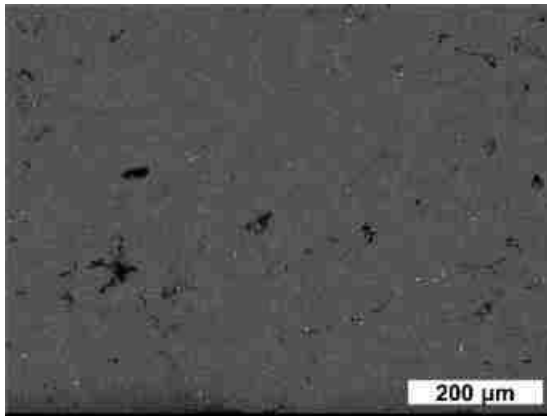
(b)
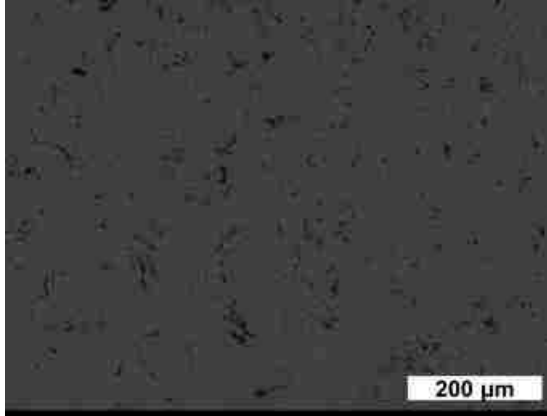
(c)

Figure 4.1 SEM micrographs showing porosity in the die cast AZ91 alloy with section thicknesses of

(a) 2 mm, (b) 6 mm, and (c) 10 mm.

The porosity contents of the HPDC AZ91 alloy specimens with the section thicknesses of 2 mm, 6 mm and 10 mm are presented in Figure 4.2. The 6 and 10 mm specimens have the high porosity contents of 2.61 % and 3.57 %, respectively, while there is a very low porosity content of only 0.53% in the 2 mm coupon. Examination of the measured porosity contents reveals the variation in casting quality resulting from differences in section thicknesses. When the casting section becomes thin, the porosity content of the HPDC AZ91 alloy decreases, and the size of the entrapped pores reduces.

The rapid cavity filling of liquid metal into the die and high solidification rates lead to the formation of the small pores and the low content of porosity in the 2 mm coupon. The implication from computer simulation of mold filling and heat transfer of the HPDC AZ91 alloy indicates that the existence of high porosity contents in the thick 6 and 10 mm specimens might be attributed to the improper filling pattern and slow solidification [10].
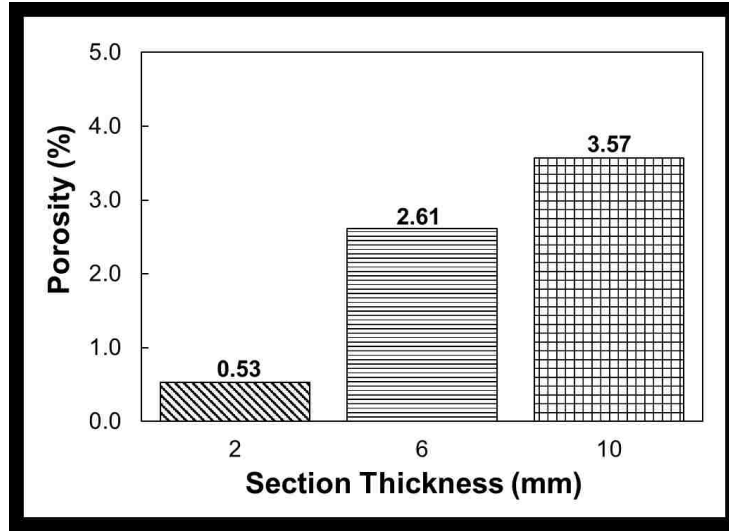
Figure 4.2 Porosity content vs. section thicknesses

4.3.2 Dendrite Measurement

Figure 4.3 gives SEM micrographs showing the existence of a fine microstructure in the outer skins of the HPDC AZ91 alloy for the 2, 6 and 10 mm specimens. The dendrite sizes in the outer skins of the HPDC AZ91 alloy are 6, 15 and 20 µm for the 2, 6 and 10 mm specimens, respectively. The dendritic structure in the center of the AZ91 coupons are present in Figure 4.4. It can be seen from Figure 4.4(a) that the dendrite size in the center of the 2 mm is only 14 µm and still small. However, there are large primary α-Mg dendrites (32 µm) in the center of the 10 mm specimen. Figure 4.5 summarizes the average size of primary α-Mg dendrites in different region of each section thickness. The reduction in the section thickness decreases the dendrite size considerably, although the variation of the dendritic structure is insignificant in the outer skins.
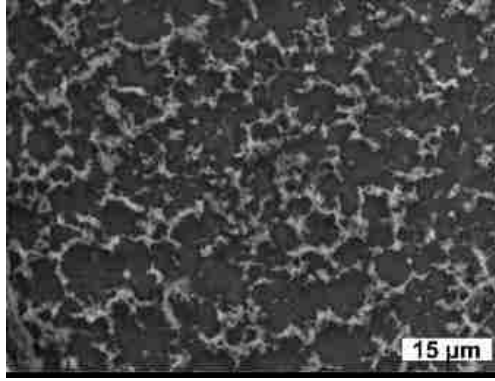
(a)
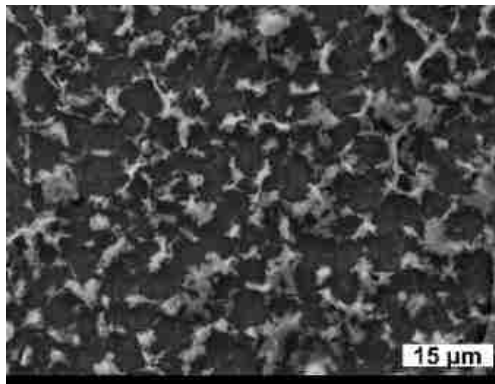
(b)
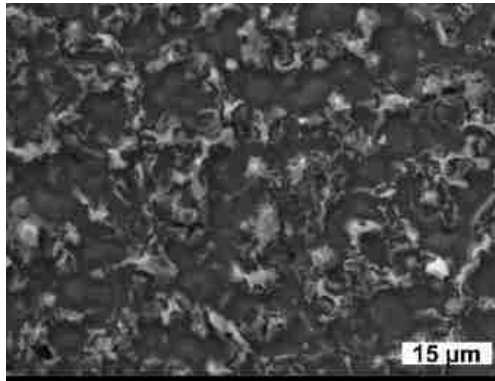
(c)

Figure 4.3 SEM micrograph showing microstructure in the outer skin of the die cast AZ91 alloy with

difference wall thicknesses, (a) 2, (b) 6 and (c) 10 mm, respectively
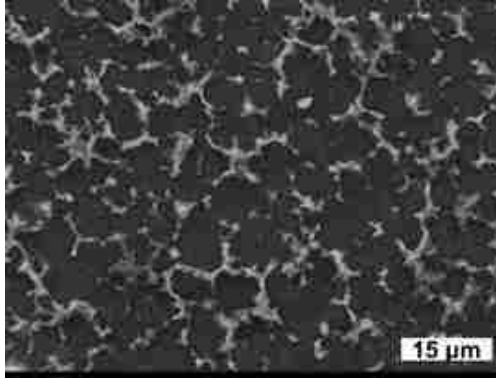
(a)
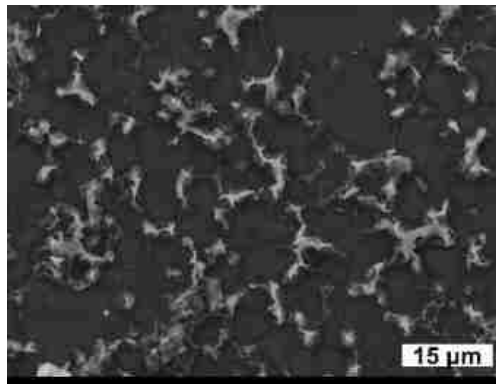
(b)
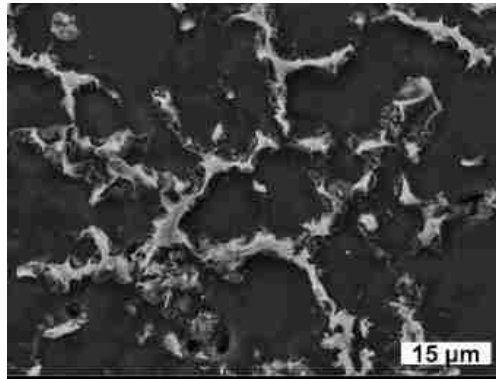
(c)

Figure 4.4 SEM micrograph showing microstructure in the center of the die cast AZ91 alloy with

difference wall thicknesses, (a) 2, (b) 6 and (c) 10 mm, respectively.
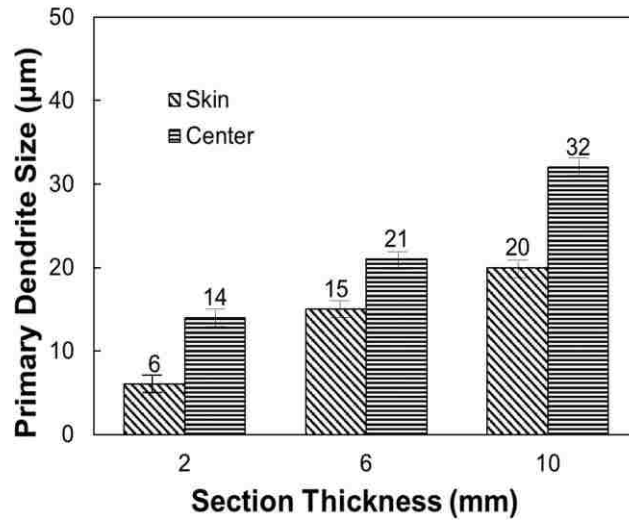
Figure 4.5 Average primary dendrite size in the out skin and center of the die cast AZ91 alloy with the section thicknesses of 2, 6 and 10 mm.

The relation between the skin thickness in the skin area, and section thicknesses is shown in Figure 4.6. With the section thickness increase, more gas is entrapped into the die and the tendency to form shrinkage porosity is also become high. As the die temperature is constant for all three thicknesses coupons, the cooling rate is almost the same for all three coupons at the very beginning of solidification. As solidification keeps on going, the thicker specimen tends to release more latent heat, which reduces the solidification rate. As a result, more shrinkage porosity and thinner skin tends to form in the thick specimens.
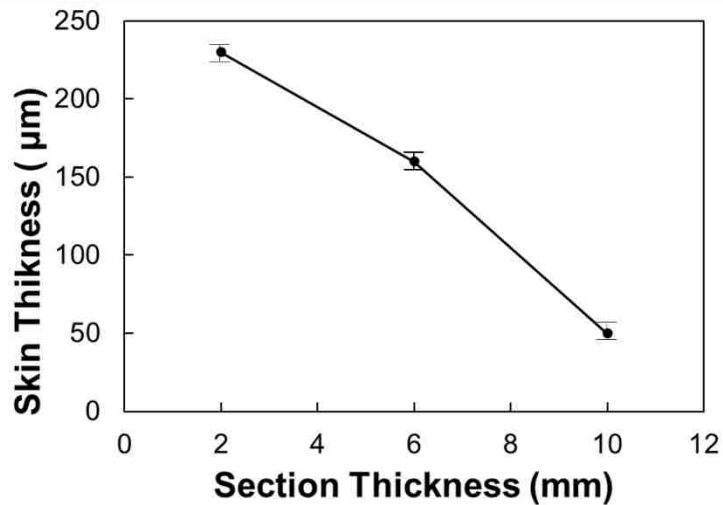
Figure 4.6 Skin Thickness vs. Section Thickness

To understand the development of the observed microstructure of the HPDC AZ91, the filling and solidification sequences of the conventional HPDC process need to be taken into consideration. The process starts with pouring the liquid metal at a desired temperature into a shot sleeve. The direct contact between the liquid metal and the sleeve chills the metal rapidly to its liquidus temperature and kicks off solidification. The formation of a large volume fraction of the primary α-Mg dendrite occurs in the sleeve prior to the metal arrives at the gate of the die cavity. Once the partially-solidified metal is pushed into the cavity, the pre-formed α-Mg crystals floats in the melt, which stays in the finally-solidified microstructure [5]. Due to the fast cooling at the interface between the casting and die, the surface of the specimens become the location to form fine grains. In the center of the specimens, the solidification for the 6 and 10 mm thick specimen due to their thick section thickness takes place much more slowly than that of the 2 mm specimen. As a result, the coarse microstructure developed in the center of the 10 mm thick specimen.

4.3.3 Eutectic Content

Figure 4.7 presents the SEM images in BSE mode showing the etched microstructure of the AZ91 alloy in details at a high magnification. The results of the EDS analysis as shown in Figure 8 and the element analysis in atomic percentages listed in Table 4.1 indicate that the microstructure of the etched AZ91 consists of primary α-Mg grains (dark), eutectic β-$Mg_{17}Al_{12}$ phases (bright), and Al-Mn intermetallics (white spot). The eutectic β-$Mg_{17}Al_{12}$ phases and Al-Mn intermetallics are present in the form of isolated fine particles surrounding the boundaries of the primary α-Mg grains.
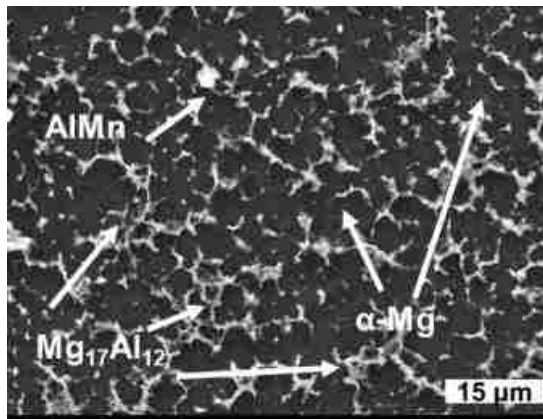
(a)
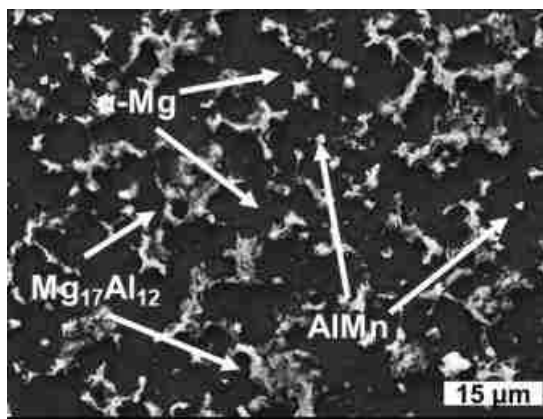
(b)
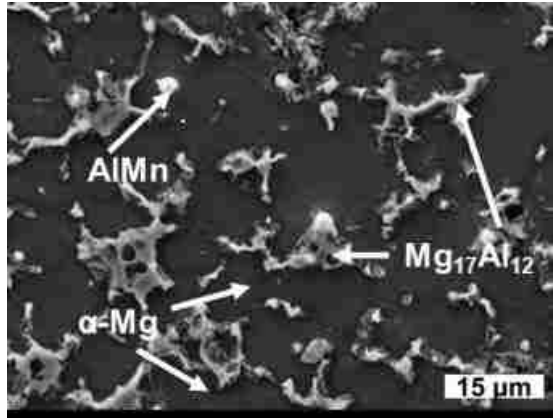
(c)

Figure 4.7 SEM micrographs in BSE mode showing constituent phases in the microstructure of the die

cast AZ91 alloy (a) 2, (b) 6 and (c) 10 mm.
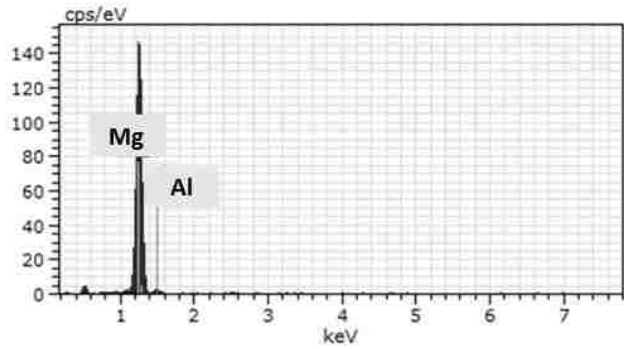
(a)
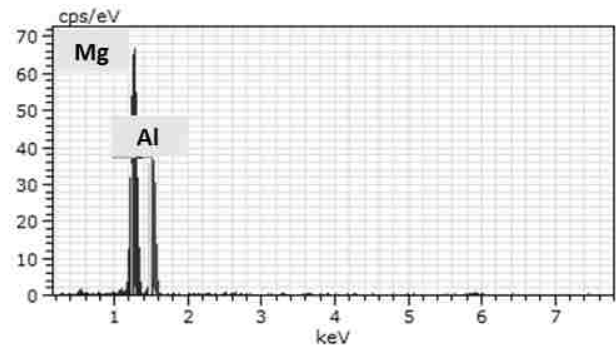
(b)
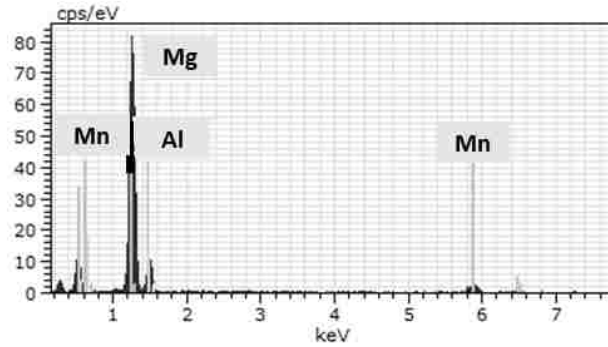
(c)

Figure 4.8 EDS spectra (a), (b) and (c) for the areas containing α-Mg grains (dark), and β-Mg17Al12
phases (bright), and Al-Mn intermetallic (white spots) as shown in Figure 4.7, respectively.

Table 4.1 Elements in analyzed phases shown in Figure 4.5

Phase	Element	Atomic (at. %)
α-Mg	Mg	96.68
	Al	3.32
$Mg_{17}Al_{12}$	Mg	57.15
	Al	42.85
AlMn	Mg	56.57
	Al	26.48
	Mn	16.95

Figure 4.9 presents the converted micrographs from Figure 4.7, highlighting the
presence of the $Mg_{17}Al_{12}$ eutectics in the observed alloys represented by the black area.
Shown in Figure 4.9, the image analysis reveals that the volume fraction of the
intermetallic phases decreases with increasing the section thickness. Figure 4.10 shows
the variation of the volume fraction of the eutectics with the different section thickness.

64

The volume fractions of the intermetallic phases in 2, 6 and 10 mm are measured to be 19.86%, 16.71% and 14.91%, respectively.
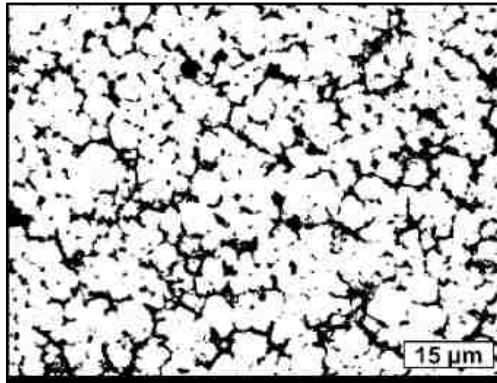
(a)
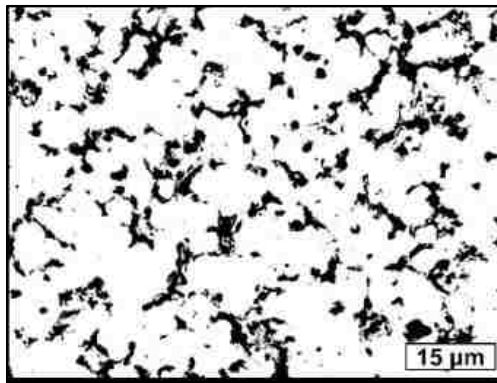
(b)
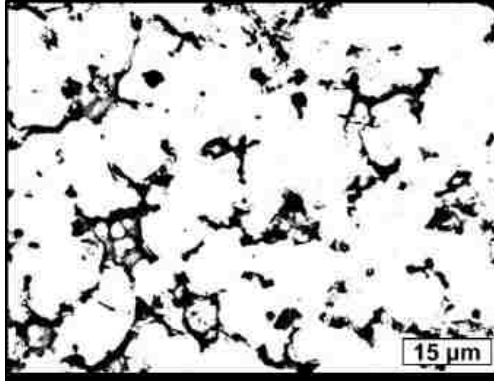
(c)

Figure 4.9 Binary black and white images showing the eutectic contents in the die cast AZ91 alloy

with the section thicknesses, (a) 2, (b) 6 and (b)10 mm, respectively.
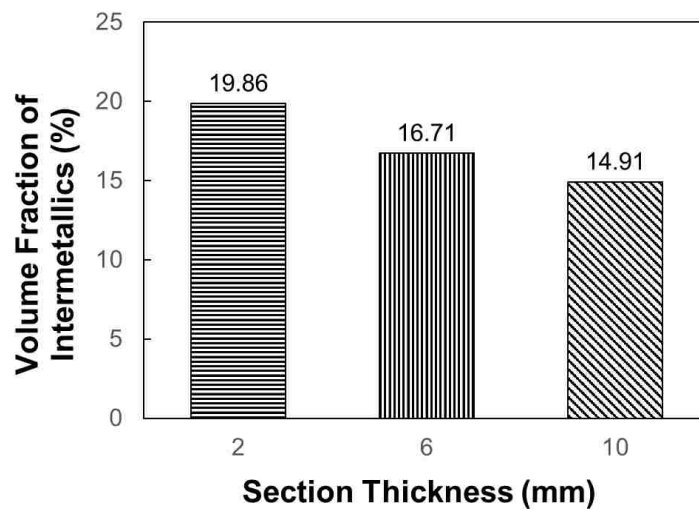
Figure 4.10 Volume fraction of eutectics varying with the section thickness

4.3.4   Tensile Properties

The variation of engineering tensile properties including UTS, YS, e_f, tensile

toughness and resilience with the section thicknesses are compiled in Table 4.2. The UTS

and YS decreases to 129 and 110 MPa for 10 mm thick specimens; from 245 and 169

MPa for the 2 mm coupons, which implies over 50% reduction in UTS and almost 35%

decrease in YS, respectively. Moreover, the elongations are 4.07%, 3.04% and 0.73% for

66

the 2, 6, and 10 mm specimens, respectively, indicate evidently that a significant decrease in elongation occurs when the section thickness of specimens increases. The results of the current study is consistent with the relationship between tensile properties and section thicknesses for different types of die casting magnesium alloys reported in the literature [7-9]. As mentioned above, differences in the porosity level and the microstructure of die cast AZ91 should be responsible for the deviation in strengths and elongation. The fine dendritic structure, high volume fractions of eutectics and low porosity level of the thin specimens enhances their tensile properties. The relatively low strengths and elongations of the thick specimens result from the coarse dendritic structure, low volume fractions of eutectics, thin skin layer, high porosity level in the center, and the presence of large pores.

Table 4.2 Tensile Properties of the die cast AZ91 alloy at room temperature

Section Thickness (mm)	UTS (MPa)	YS (MPa)	e_f (%)	Young's Modulus (GPa)
2	245.54±5.65	169.26± 5.48	4.07±0.34	37.8±2.26
6	182.91±4.75	132.02±3.95	3.04±0.18	28.6±1.43
10	129.17±7.11	110.59±6.82	0.73±0.21	25.9±1.30

4.3.5 Deformation Behavior

(1) Resilience

The ability of a material to absorb energy is referred to as resilience when it is deformed elastically and releases that energy upon unloading. The resilience is usually measured by the modulus of resilience which is defined as the maximum strain energy absorbed per unit volume without creating a permanent distortion. It can be calculated by

integrating the stress-strain curve from zero to the elastic limit. In uniaxial tension, the strain energy per unit volume can be determined by the following equation:

$$U_r = \frac{(YS)^2}{2E}$$
Equation 4.3

where U_r is the modulus of resilience, YS is the yield strength, and E is the Young's modulus. The calculated moduli of resilience for different section thickness of AZ91 are given in Table 4.3. In comparison between 2 mm and 10 mm specimens, the modulus of resilience in 2 mm is 140 kJ/m^3 higher than that of the 10 mm. This implies that the AZ91 in the 2 mm thickness is much more capable of resisting energy loads in engineering application during service, in which no permanent deformation and distortion are allowed.

(2) Toughness

The tensile toughness of a ductile alloy is its ability to absorb energy during static loading condition, i.e., static deformation with a low strain rate. The ability to bear applied stresses higher than the yield strength without fracturing is usually required for various engineering applications. The toughness for ductile alloys can be considered as the total area under the stress-strain curve for the amount of the total energy per unit volume. To evaluate the deformation behavior, the energy expended in deforming a ductile alloy per unit volume given by the area under the stress-strain curve can be approximated by

$$U_t = U_{el} + U_{pl} = \frac{(YS+UTS)}{2} \times e_f$$
Equation 4.4

where U_t is the total energy per unit volume required to take to point of fracture, U_{pl} is the energy per unit volume for elastic deformation, and U_{el} is the energy per unit

68

volume for plastic deformation, and e_f is the elongation at fracture. Table 4.3 lists the calculated values of the U_t for AZ91 with different section thickness. Examination of the U_t values reveals that the 2 mm specimen exhibits an U_t value of 8.34 MJ/m^3 higher than the 6 mm and the 10 mm specimen. This is because the 2 mm AZ91 alloy has a higher ultimate tensile strength and a greater elongation. As a result, the total area under the stress and strain curve is much larger for the 2 mm specimen.

Table 4.3 Tensile toughness and resilience of die cast AZ91 at room temperature

Section Thickness (mm)	Toughness (MJ/m^3)	Resilience (kJ/m^3)
2	8.34±0.57	378.95±15.45
6	4.78±0.62	304.71±18.23
10	0.89±0.05	236.10±12.85

(3) Strain Hardening

Figure 4.11 shows the representative true stress and strain curves of the die cast AZ91 alloy. For all three section thicknesses of specimens, the stress variation with the strain follows almost the same pattern. Under tensile loading, the alloy deformed elastically first. Once yield points reach, plastic deformation of the alloy sets in. However, the fracture of the 2 mm-thick specimen occurs at a much higher stress and elongation than that for the 6 and 10 mm thick specimens.
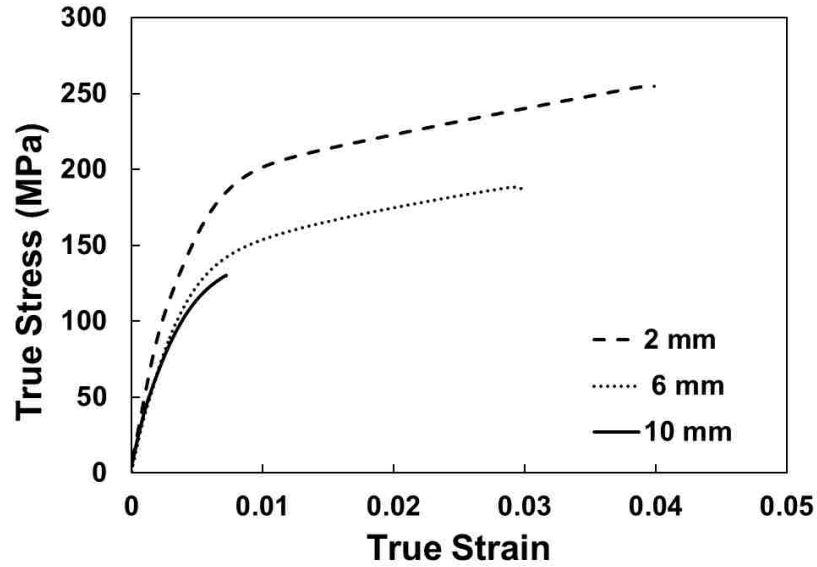
Figure 4.11 Typical true strain vs. stress curves for the die cast AZ91 alloy.

The stress-strain curve for metals is often described by the power expression

$$\sigma = K\varepsilon^n \qquad \text{Equation 4.5}$$

where σ is the true stress, K is the strength coefficient, ε is the true strain and n is the strain hardening exponent. The regression analysis indicates that the power expression is in a reasonable agreement with the tensile results. The numerical values of these constants in Equation 4.5 with the regression coefficients (R^2) are listed in Table 4.4. Equation 4.5can be differentiated to obtain strain-hardening rates ($d\sigma/d\varepsilon$).

Table 4.4 Best fits parameters for power equations

Section Thickness (mm)	K (MPa)	n	R^2
2	449.58±5.71	0.1776±0.0051	0.96±0.02
6	388.66±5.83	0.2039±0.0063	0.98±0.02
10	386.51±8.64	0.2208±0.0081	0.99±0.01

The strain-hardening behaviors of the die cast AZ91 alloy are illustrated in a plot of strain-hardening rate ($d\sigma/d\varepsilon$) vs true plastic strain (ε) during the plastic deformation as shown in Figure 4.12, which is derived from Figure 4.11. The 2 mm specimen has a high strain hardening rate (5500 MPa) with respect to that of the thick 10 mm specimen (4600 MPa) at the onset of plastic deformation. It is evident that, despite of decreasing with an increase in true strain, the strain-hardening rates during the plastic deformation of the die cast alloys varies with their section thicknesses. As the section thickness decreases, the strain hardening rates increase. This observation implies that, compared to the 6 and 10 mm thick samples, the die cast AZ91 alloy with the thin cross section (2 mm) is capable of spontaneously strengthening itself increasingly to a large extent, in response to extensive plastic deformation prior to fracture. The low porosity level and the even dispersion of fine intermetallic particles inside grains and around ground boundaries observed by Zhou et al [11], which resist slip in the primary phase should be responsible for the relatively high strain-hardening rate of the thin alloy in the early stage of plastic deformation, i.e., instantly after the onset of plastic flow as indicated in Figure 4.12.
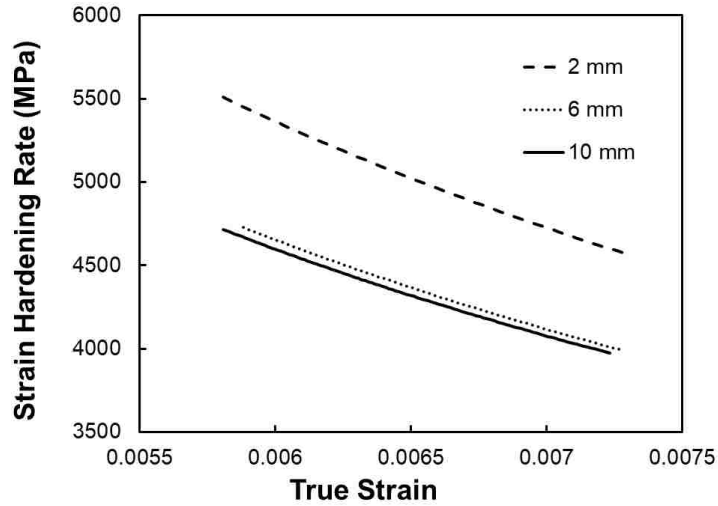
Figure 4.12 Strain hardening rate vs. true strain for plastic deformation of the die cast AZ91 alloy.

4.3.6   Fracture Characteristics

Examination of the fracture surfaces of tensile specimens via SEM manifests the fracture behavior of die cast AZ91 with three different thicknesses, which is shown in Figures 4.13-15. The circled areas are observed under a high magnification in an attempt to reveal detailed features of fracture surface and determine the manner where the primary crack originated. The analysis of SEM fractography shows that the fracture behavior of die cast AZ91 is influenced by the section thicknesses. As the section thickness increases, the fracture of AZ91 tends to transit from ductile to brittle mode.

The fracture surface of the 2 mm thick specimen illustrated in Figure 4.13 is primarily ductile in nature, which is characterized by the presence of deep dimples. The fractograph with a higher magnification, Figure 4.13 (b), portrays the dimples with extensive deformation marking along the walls of individual craters. A considerable amount of energy is consumed in the process of the formation of microvoids and microvoid-sheet, eventually leading to the creation of cracks. Thus, this type of fracture failure results from the coalescence of microvoids under the tensile stress. It seems,

72

however, that the failure of the 10 mm-thick specimen is caused by a combined brittle fracture mechanism of void coalescence and intergranular fracture (Figure 4.15). The similar mechanism for the fracture of die cast magnesium alloys has also been reported in references 11 and 12.

(a)

(b)
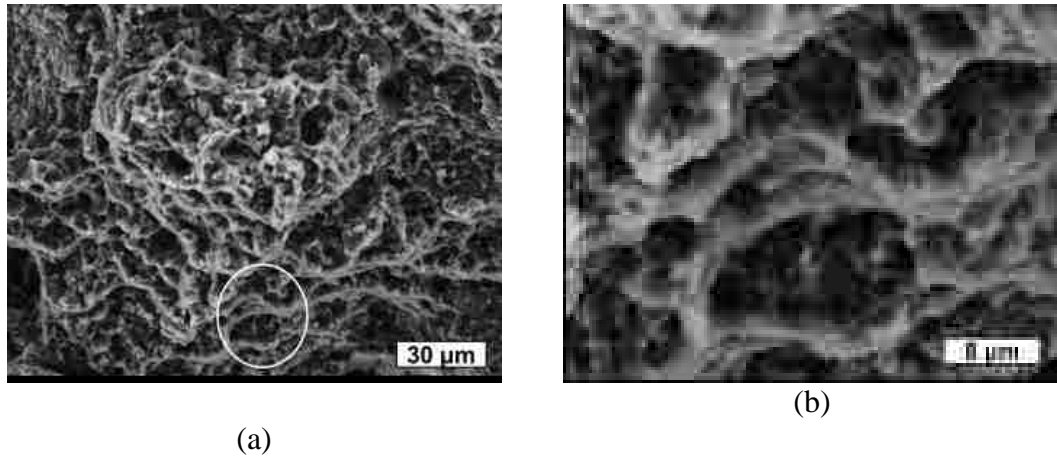
Figure 4.13 SEM fractographs of the 2 mm-thick die cast coupon, (a) low and (b) high magnifications.

(a)

(b)
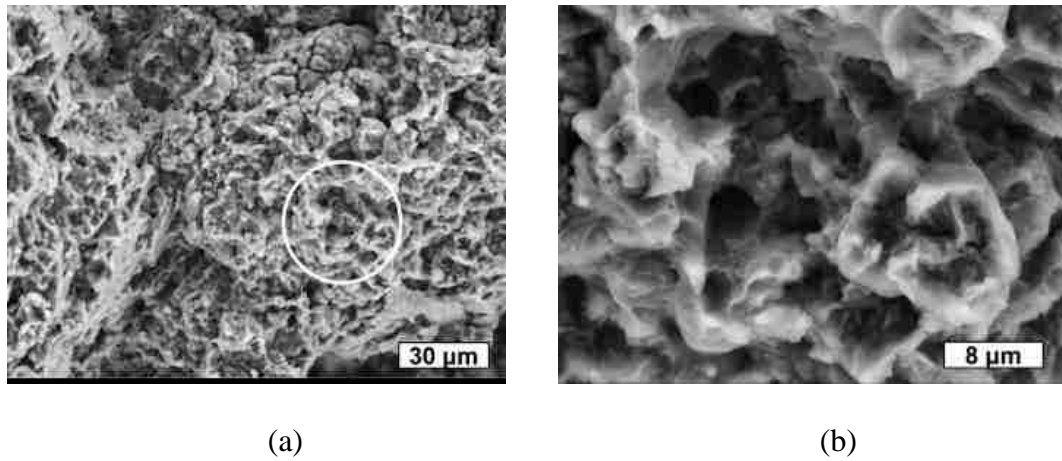
Figure 4.14 SEM fractographs of the 6 mm-thick die cast coupon, (a) low and (b) high magnifications
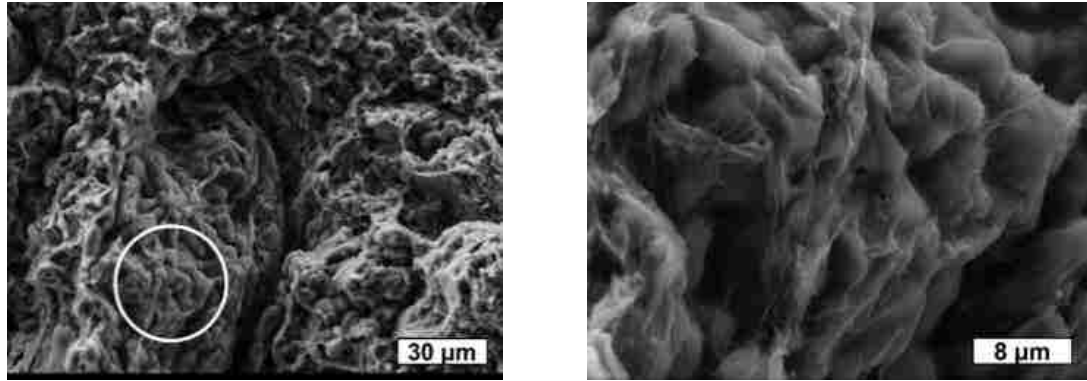
| (a) | (b) |

Figure 4.15 SEM fractographs of the 10 mm-thick die cast coupon, (a) low and (b) high magnification.

The strain-hardening and fracture failure of the high pressure die cast magnesium alloy AZ91 is influenced by its section thickness. The results of tensile testing indicate that the mechanical properties, UTS, YS, and e_f, as well as resilience (U_r) and toughness (U_t) increase significantly with a reduction in the section thickness of the alloy. The analysis of plastic deformation behavior reveals that, an increase in high strain-hardening rates of the alloy with decreasing the section thickness enables the alloy to spontaneously strengthen the materials increasingly to a large extent, in response to extensive plastic deformation prior to fracture. The observation via SEM fractography illustrates that the fracture behavior of die cast AZ91 is influenced by the section thickness. As the section thickness increases, the fracture of AZ91 tends to transit from ductile to brittle mode.

74

[1] K. Guan, B. Li, Q. Yang, X. Qiu, Z. Tian, D. Zhang, D. Zhang, X. Niu, W. Sun, X. Liu and J. Meng, "Effects of 1.5wt% samarium(Sm) addition on microstructures and tensile properties of a Mg-6.0Zn-0.5Zr alloy," J. Alloys and Compounds Vol. 735, pp. 1737, 2018.

[2] Y.Y Li, W.M. Zhao, J. Ding and H.T. Xue, "Ignition-proof performance and mechanism of AZ91D-3Nd-xDy magnesium alloys at high temperatures" China Foundry Vol.15 No.2 (2018), pp. 97, 2018.

[3] B.R. Powell, V. Rezhets, M.P. Balogh and R.A.Waldo, "Microstructure and creep behavior in AE42 magnesium die-casting alloy" JOM,Vol 54, pp. 34, August 2002.

[4] A.A. Luo, "Magnesium casting technology for structural application,"Journal of Magnesium and Alloys Vol. 1, issue 1, pp. 2, March 2013.

[5] M.M. Avedesian, and H. Baker, *Magnesium and Magnesium Alloys-ASM Specialty Handbook* ,ASM Int., Materials Park, OH, USA, 1999.

[6] M. Zhou, N. Li and H. Hu, "Effect of Section Thicknesses on Tensile Behavior and Microstructureof High Pressure Die Cast Magnesium Alloy AM50,"Mater. Sci. Forum Vols. 475-479 , pp. 463, 2005.

[7] C.H. Cáceres, W.J. Poole, A.L. Bowles and C.J. Davidson, "Section thickness, microhardness and yield strength in high -pressure diecast magnesium alloy AZ91" Materials Science and Engineering A,Vol. 402 *Issues* (1-2) , pp. 269, August 2005.

[8] S.L. Sin, D. Dubé and R. Tremblay, "An investigation on microstructural and mechanical properties of solid mould investment casting of AZ91D magnesium alloy," Materials Characterization Vol. 59, Issues (2) , pp.178, February 2008.

[9] Haavard T. Gjestland, Stian Sannes, Hakon Westengen, Darryl Albright, "Effect of Casting Temperature, Section Thickness and Die Filling Sequence on Microstructure and Mechanical Properties of High Pressure Die Castings" Dies Casting Engineering, Vo.l48, No.4, pp.56, 2004

[10] M. Zhou, "An experimental study of die and squeeze cast magnesium alloy AM50,"M.S. thesis, Dept. Mechanical, Automotive, and Material, Univ. of Windsor, Windsor, Ontario, Canada, 2004.

[11] Z. Sun, M. Zhou, N, Li, and H. Hu, "Strain-Hardening and Fracture Behavior of Die Cast Magnesium Alloy AM50," *Adv.Mater.SCI ENG* 2007.

[12] M. Zhou, N. Li, J. Lo, and H. Hu, "Microstructure and tensile properties of squeez cast magnesium alloy AM50," *J.Mater.Eng.Perform.*Vol. 14, No. 4, pp. 539, 2005

██ ████████████

Magnesium alloys have great properties that suit numerous applications. Their high strength to weight ratio, good castability, and low density attract interests of many industries. Especially, in the fields of automotive and aerospace, the researches of increasing the fuel efficiency have been continuedly studied. It is crucial that the proper design of structural application maximizes the usage of light weight material to improve fuel efficiency. In certain applications, magnesium and its alloys can perform the same engineering functionality at low mass compared with competitive materials such as steel and aluminum. However, poor corrosion resistant of magnesium alloys confines their range of uses [1]. Particularly in corrosive environments, mechanical properties of magnesium and its alloys decrease as their exposure extends. A suitable surface treatment may enhance corrosion resistance. Plasma electrolyte oxidization (PEO) is a promising coating technology which is widely used in mechanical and biological engineering due to the low cost, high efficiency and environment friendliness [2]. The magnesium alloy with eco-friendly PEO coating create components which still have low density, but with inproved corrosion resistance. On the topic of plasma electrolytic oxidation coating, major focus is on its corrosion resistant aspect. Although previous studies show that the PEO coating significantly increases corrosion resistant of magnesium alloys [3], the effect of PEO coating on mechanical properties remains uncleared. Few researchers have studied the effect of PEO coating on stress corrosion cracking and fatigue performance [4-6]. Hu and Nie [7] performed tensile tests on squeeze cast pure magnesium with and

77

without PEO coating. Their tensile testing results show that a thin PEO coating (7 μm) decreases the yield strength (YS) of 3 mm thick samples, but has little effect on the ultimate tensile strength (UTS) and elongation. The study by Sun et al. [8] reveals that the UTS, YS, and elongation of the high pressure die cast AZ91 alloy without coating decrease with increasing section thickness of magnesium alloys [8]. Thus, the correlation between section thickness, effect of PEO coating, and tensile properties for HPDC magnesium alloy AZ91 is still unknown. In this study, the PEO process was utilized to deposit coating on high pressure die cast magnesium alloy AZ91 with the section thicknesses of 2, 6, and 10 mm. The work includes an in-depth analysis of tensile properties, strain-hardening behaviour during plastic deformation, and microstructure of the PEO-coated HPDC AZ91 alloy with the section thicknesses of 2, 6 and 10 mm. The influence of PEO coating on tensile properties and plastic deformation behaviour of the alloy was investigated based on the analyse of engineering stress-strain relation and true stress-strain relation. The microstructure of the PEO coated HPDC AZ91 was characterized by using scanning electron microscopy. The fractured surface of the PEO coated AZ91 alloy was also analysed by SEM fractography.

5.2.1   Alloy and Casting Preparation

The magnesium alloy selected in this study was die casting Mg-8.48 wt.%Al-0.61 wt.%Zn-0.18 wt.% Mn alloy AZ91. Flat rectangular coupons of 125 mm × 27 mm with different section thicknesseses of 2, 6 and 10 mm were die cast on a 700 ton cold chamber horizontal high pressure die casting machine.

5.2.2 Electrolyte Preparation and PEO Process

Prior to conducting PEO coating process, AZ91 alloy tensile samples were sanded using the abrasive paper following by 240 grits, 400 grits, and 800 grits respectively and cleaned by ultrasonic with ethanol. Then the samples (anode) was immersed in electrolyte (10 g/L $NaAlO_2$, 4 g/L Na_3PO_4, and 1 g/L KOH) in a stainless steel vessel (cathode). A bipolar pulsed ($f = 200$ Hz) direct current (dc) power supply was used. The current density was set to 0.075 A/cm^2 and voltage was kept at 480 V for 600s. After removal from the electrolyte, all samples were dried at room temperature.

5.2.3 Tensile Testing

The mechanical properties of the coated and uncoated AZ91D alloy with the section thickness of 2, 6 and 10 mm were evaluated by tensile tests, which were performed at ambient temperature on an Instron machine equipped with a computer data acquisition system. Following ASTM B557, subsize flat tensile specimens (25 mm in gage length, 6 mm in width, and 2, 6, 10 mm in as-cast thicknesses) were machined from the die cast coupons. The tensile properties, including 0.2% yield strength (YS), ultimate tensile strength (UTS), and elongation at fracture (e_f), were obtained based on the average of three tests.

5.2.4 Characterization of Microstructure

Specimens were sectioned, mounted, and polished from the center of the coupons and prepared following the standard metallographic procedures. An etchant of 60% ethanal-20% acetic acid-19% distilled water-1% nitric acid was applied to polished specimens for microscopic examination. The detailed features of the microstructure were characterized at high magnifications by a scanning electron microscope (SEM), Hitachi Tabletop

Microscope TM3000, with a maximum resolution of 30 nm in a backscattered mode (BSE)/1 µm in x-ray diffraction mapping mode, and useful magnification of 10–30,000.
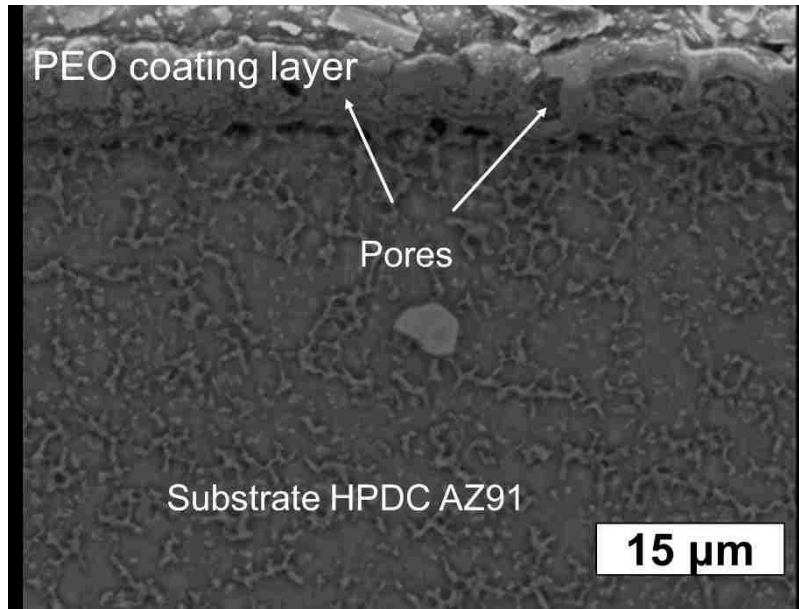
5.3.1   Microstructure

SEM images showing the morphology of the PEO coating on AZ91D magnesium alloy are presented in Figure 5.1. Overall, the coating thickness exhibits consistency throughout all three samples which is approximately 7.5 µm on each side. With the same coating thickness, the coated thin specimens proportionally contain the volume fraction of coating higher than those of the thick ones. This observation implies the PEO on thin specimens coating should be able to carry more loads than those on the thicker samples during tensile testing. Figure 5.1 also shows the different level of porosities in the substrate AZ91 alloy of the coated 2, 6 and 10 mm specimens. The porous nanostructure of the ceramic PEO coatings on the 2, 6 and 10 mm specimens is revealed under the high magnification of SEM observation as illustrated in Figure 5.2. The average size of the pores in both coatings and substrates of the 2, 6, and 10 mm specimens are given in Figure 5.3(a), which are 2.5 and 10 µm for the 2 mm, 2.7 and 31 µm for the 6 mm, and 2.4 and 72 µm for the 10 mm, respectively. The porosity percentage of the coatings and substrate are displayed in Figure 5.3(b), which are 2.97% and 0.53% for the 2 mm, 3.01% and 2.61% for the 6 mm, and 2.95% and 3.57% for the 10 mm. All the coatings on the three different thickness specimens contain both nano-size and micron-sized pores. In the 2 mm sample, the pores presented in the ceramic coating could serve as sites for crack initiation, since the substrate is basically free of porosity. There are the visible pores in both the coating and the substrate of the coated 6 mm specimen (Figure. 5.1(b)). Similar

to that of the 6 mm specimens, the pores are evidently present in both the coating and the substrate of the 10 mm specimen as shown in Figure 5.1 (c). However, the percentage and size of the pores in the substrate of the 10 mm specimen are much higher and larger than those in 6 mm specimen.

The comparison of the pore structure between the 6 and 10 mm specimens suggests that the pores in the coating of the 6 mm one might still play a significant role in initiating and growing crack due to their size similar to those in the substrate. But, in the 10 mm specimen, the crack initiation and growth should be controlled by the massive presence of the large pores in the substrate, since the pores in the coating are much smaller. The presence of a relatively dense PEO coating on the very porous substrate of the 10 mm specimen could be protective and prevent the crack initiation as well as slow down the crack growth, which results from the massive presence of the large pores in the substrate.

Additionally, during the PEO coting process, the chemical reactions take place mainly between the primary α-Mg phase and electrolytic ion solutions. The high content of large primary α-Mg dendrites present in the 10 mm specimen facilitates the formation of the uniform and continuous interface between the PEO coating and the substrate, in comparison of that in the 2 mm specimen. Figures 5.2 (a) and (b) show the presence of discontinuity in the interface of the coated 2 and 6 mm specimens. This is because the 2 mm and 6 mm specimens have the relatively high-volume fractions of the β-$Mg_{17}Al_{12}$ phase with the low content of the fine primary α-Mg dendrites, especially along the edge of the specimen, which hinders the formation of the continuous PEO crystalline structure at the interface. The continuous interface evidently exhibits in the coated 10 mm

specimen as revealed in Figure 5.2 (c). The presence of the continuous interfaces in the 10 mm specimen could mitigate crack propagation from the PEO ceramic coating inward to the substrate during tensile loading, which might improve the mechanical properties.

(a)
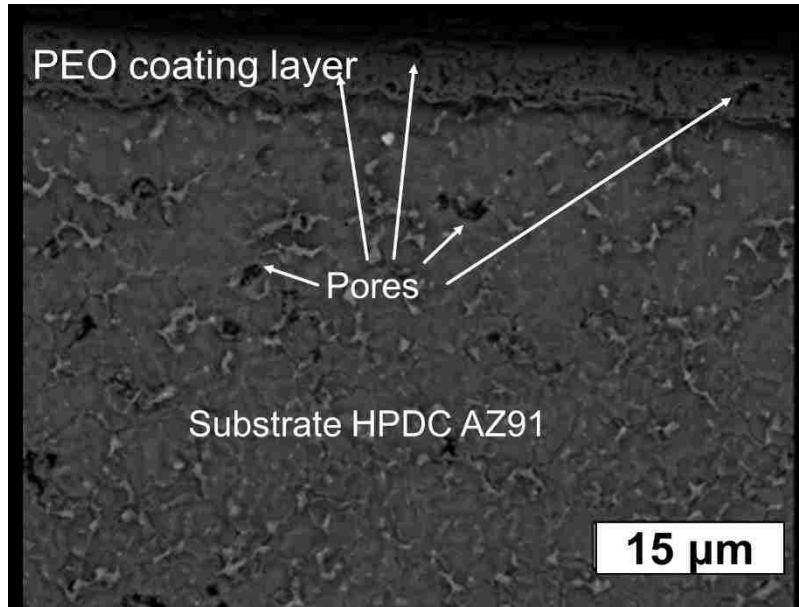
(b)
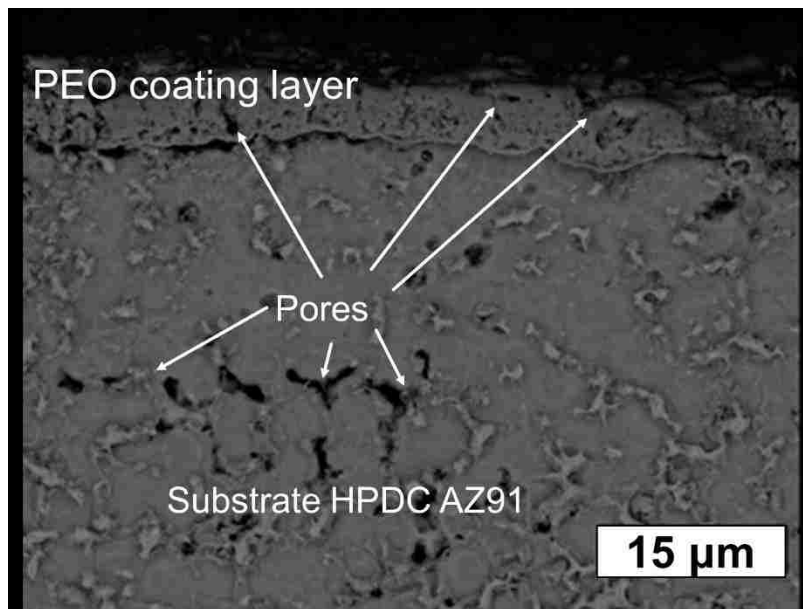
(c)

Figure 5.1 SEM micrographs showing the microstructure of the coated AZ91D alloy with the section

thicknesses (a) 2, (b) 6, and (c) 10 mm.

(a)

(b)

(c)

Figure 5.2 SEM micrographs showing the structure of the PEO coating on AZ9211 alloy with the section thickness, (a) 2, (b) 6, and (c) 10 mm.

(a)

(b)

Figure 5.3 (a) Average pore sizes and (b) Percentage of porosity in the substrate and PEO coating

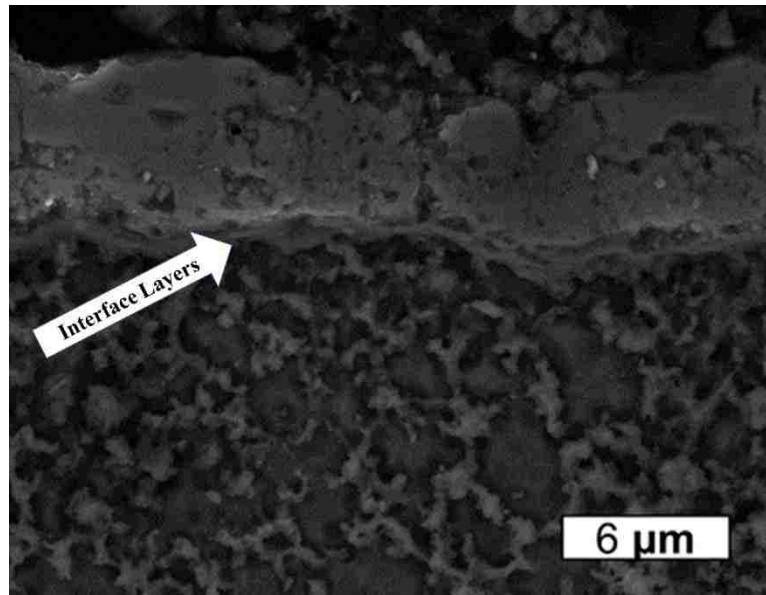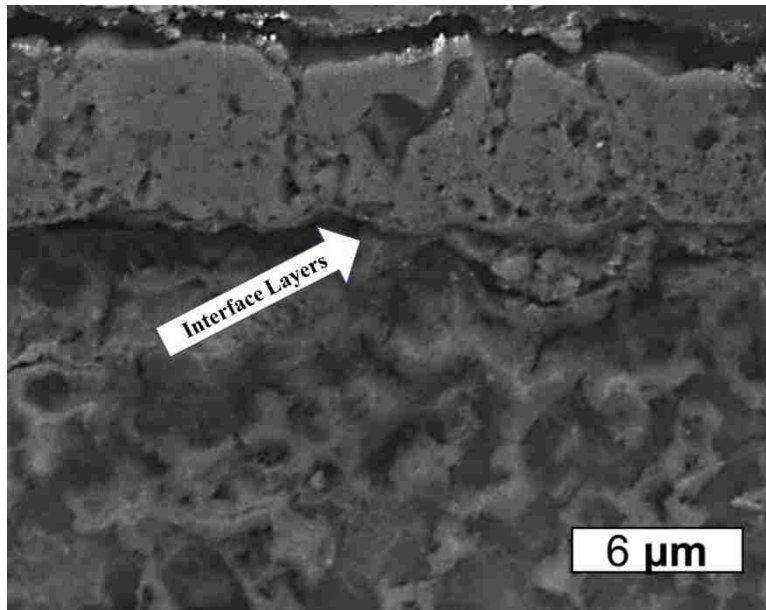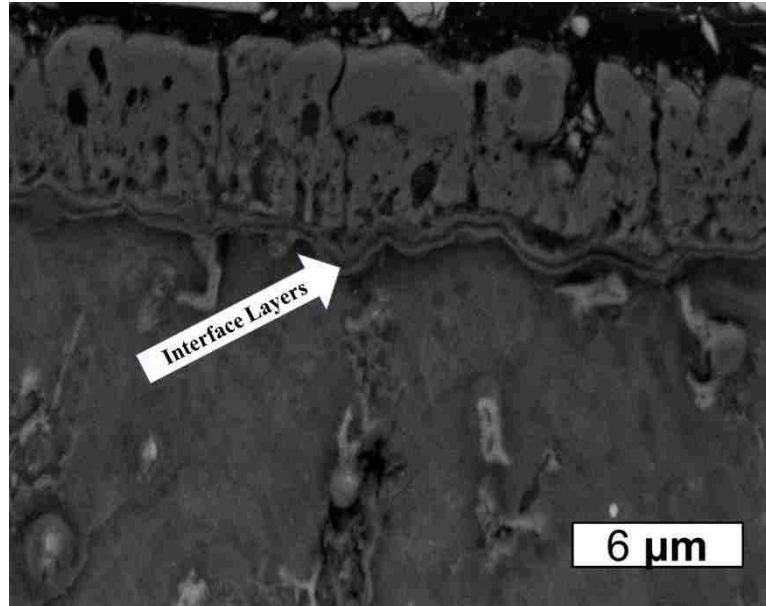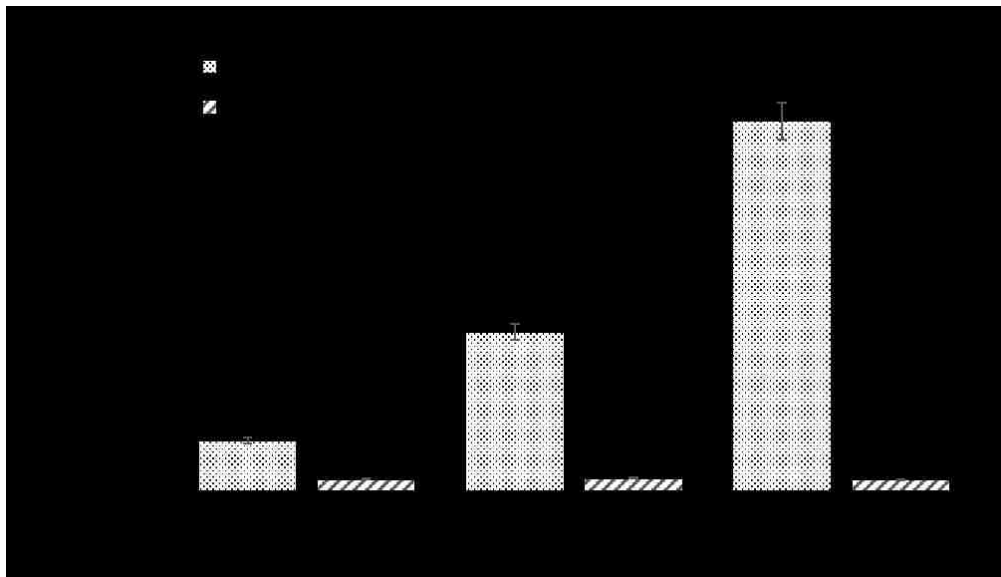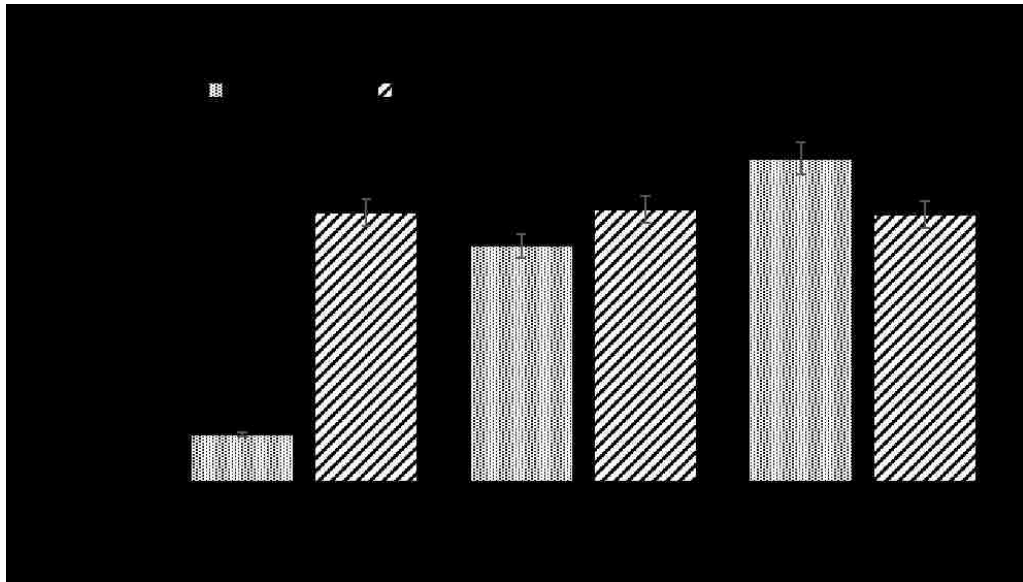layer of the HPDC Mg alloy AZ91 with the section thicknesses of 2, 6, and 10 mm.

5.3.2 Tensile Properties

To demonstrate and compare the effect of PEO coating on the tensile behavior of the HPDC AZ91 alloy, the data of the uncoated alloy was used as references [9]. Figure 5.4 shows the representative engineering stress-strain curves of both the uncoated and coated samples. The variation of engineering tensile properties including UTS, YS, and elongation with the coated section thicknesses are compiled in Table 5.1. In the groups of the 2 and 6 mm samples, compared with the uncoated tensile results, their mechanical properties significantly decrease. For the 2 mm sample, the UTS drops from 245.52 MPa to 196.61 MPa; the YS from 169.26 MPa to 139.17 MPa; the elongation reduces from 4.07% to 2.94%, which implies a reduction of 20% in UTS, 18% in YS, and 25% in elongation. The results of the 6 mm samples also reflect that the PEO coating has a negative effect on the mechanical properties of the HPDC AZ91 alloy, of which UTS, YS and elongation are reduced by 7%, 6% and 11%, respectively. On the contrast, while the uncoated 10 mm sample exhibits 129.17 MPa in UTS, 110.57 MPa in YS and 0.73% in elongation, the UTS, YS and elongation of the coated HPDC AZ91 alloy increase to 140.35 MPa (8%), 122.74 MPa (10%) and 0.75% (2%), respectively. The phase constitution, microstructure and the volume fraction ratio of the coating and substrate as discussed in the in the preceding section should be responsible for the resultant tensile results.

Table 5.1 Tensile Properties of the die cast AZ91D vs PEO coated AZ91D alloy at room temperature

Section Thickness	Surface Condition	UTS (MPa)	YS(MPa)	e$_f$ (%)
2	Uncoated	245.52 ±5.65	169.26±5.48	4.07±0.34
	PEO Coated	196.61±6.14	139.17±5.83	2.94±0.29
6	Uncoated	182.27±4.75	132.02±3.95	3.04±0.18
	PEO Coated	168.27±5.10	122.56±5.73	2.7±0.17
10	Uncoated	129.17±7.11	110.59±6.82	0.73±0.21
	PEO Coated	140.35±6.52	122.74±5.43	0.75±0.13
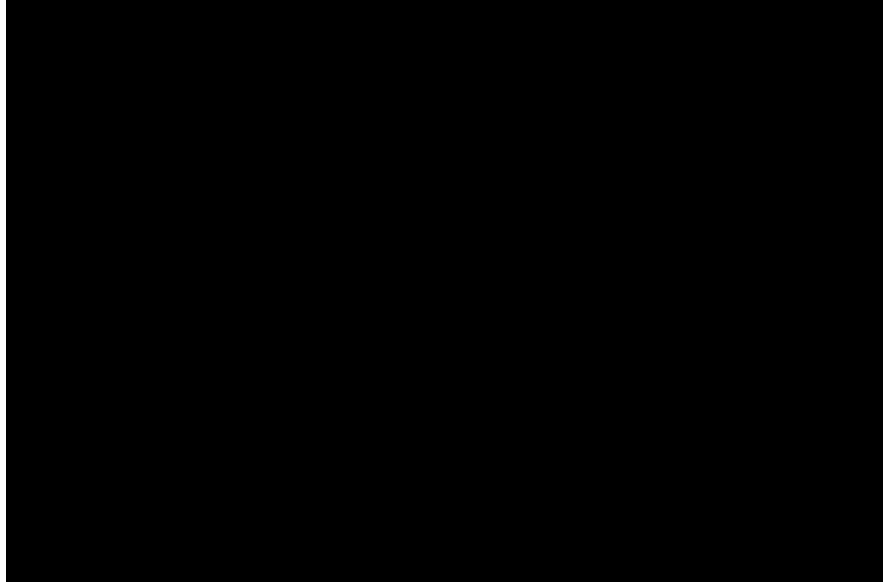
(a)
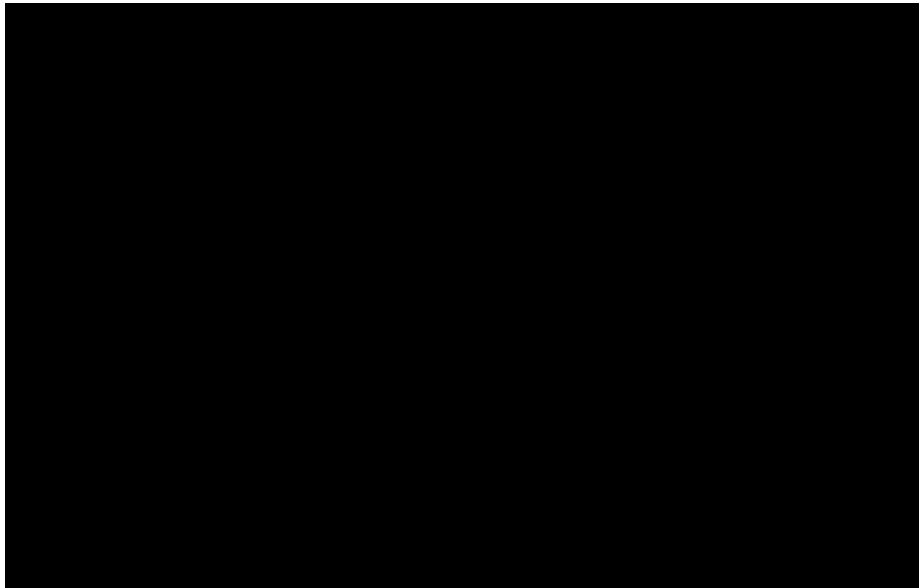
(b)
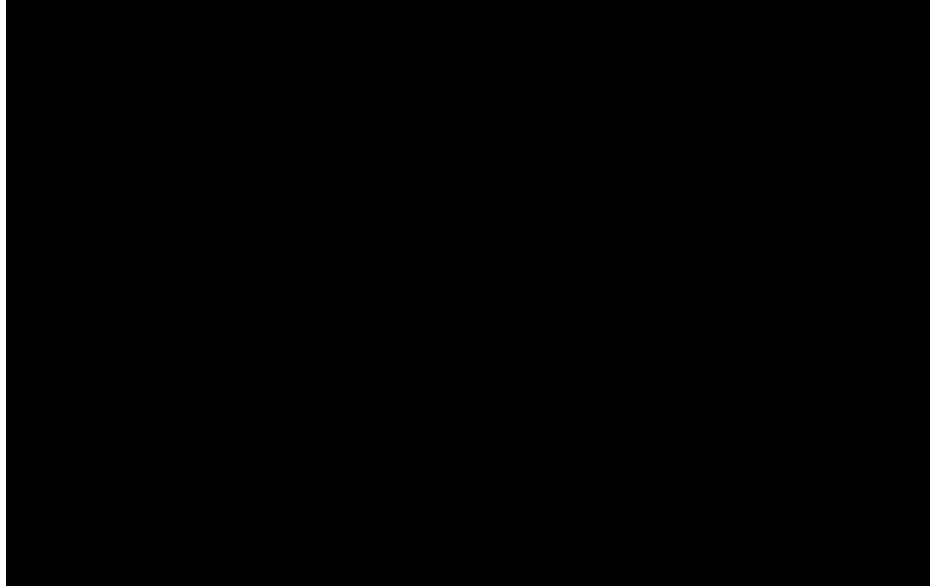
(c)
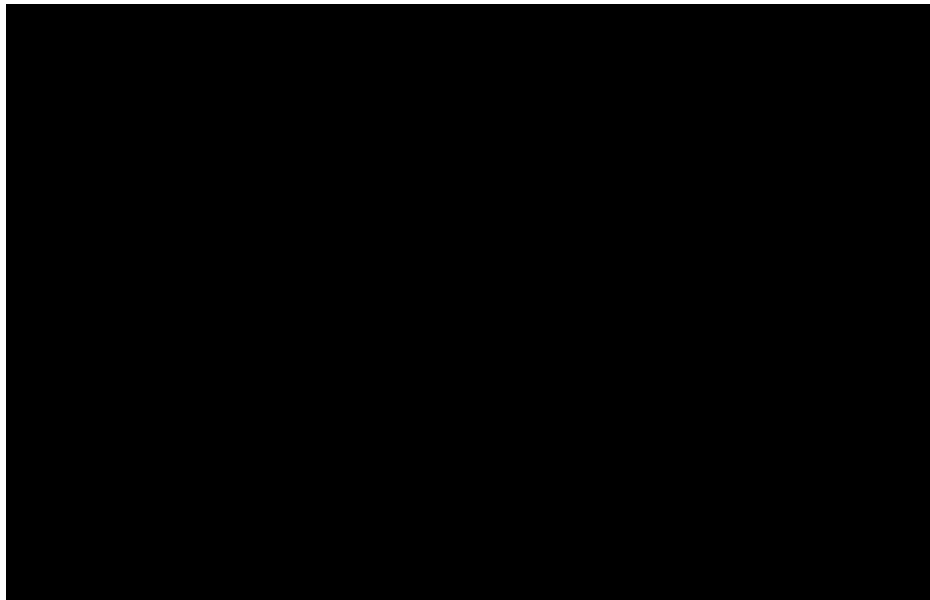
(d)

Figure 5.4 Engineering stress-strain curve of the uncoated and PEO coated (a) six curves for all the three section thicknesses and (b) 2, (c) 6, and (d) 10 mm HPDC AZ91 Alloy.

5.3.3   Modulus of Resilience and Tensile Toughness

Based on the tensile properties data, both modulus of resilience and tensile toughness were calculated. The modulus of resilience can be calculated by integrating the stress-strain curve from zero to the elastic limit. In uniaxial tension, the strain energy per unit volume can be determined by the following equation:

$$U_r = \frac{(YS)^2}{2E} \qquad\qquad \text{Equation 5.1}$$

where U_r is the modulus of resilience, YS is the yield strength, and E is the Young's modulus. To calculate the tensile toughness, the energy expended in deforming a ductile alloy per unit volume given by the area under the stress-strain curve can be approximated by

$$U_t = \frac{(YS+UTS)}{2} \times e_f \qquad\qquad \text{Equation 5.2}$$

where U_t is the total energy per unit volume required to take to point of fracture and e_f is the elongation at fracture.

Table 5.2 lists the calculated values of the U_r and the U_t for the PEO-coated and uncoated AZ91 alloy with different section thicknesses. Examination of the U_t values reveals that the coated 2 mm specimen exhibits an U_t value of 5.04 MJ/m^3 higher than the coated 6 mm (4.65 MJ/m^3) and the coated 10 mm (0.98 MJ/m$^{3)}$ specimen. However, by comparing with the uncoated results, both the 2 and 6 mm samples show reductions in toughness and resilience. For the 2 mm samples, the toughness and the resilience are decreased by 40% and the by 23%, respectively; for the 6 mm samples, the toughness and the resilience are decreased by 5% and 0.7%. On the contrary, for the 10 mm samples, the toughness and the resilience show increases by 10% and 20%. The results of the

calculated moduli and tensile toughness reveal that the outer coating layer promotes the crack initiation and growth in the thinner samples during tensile loading, which consequently reduces the capability of material energy absorption.

Table 5.2 Tensile toughness and resilience of die cast AZ91 at room temperature

Section Thickness (mm)	Surface Condition	Young's Modulus (GPa)	Toughness (MJ/m³)	Resilience (kJ/m³)
2	Uncoated	37.8±2.26	8.34±0.57	378.95±15.45
	PEO-Coated	33.2±1.98	5.04±0.31	291.69±12.89
6	Uncoated	28.6±1.43	4.78±0.62	304.71±18.23
	PEO-Coated	28.8±	4.56±0.54	302.59±16.31
10	Uncoated	25.9±1.30	0.89±0.05	236.10±12.85
	PEO-Coated	26.6±1.72	0.98±0.06	283.18±14.74

5.3.4   Deformation Behavior

Figure 5.5 shows the representative true stress and strain curves of the die cast AZ91 alloy. For all the three section thicknesses of specimens, the stress variation with the strain follows almost the same pattern. Under tensile loading, the alloy deformed elastically first. Once yield points reach, plastic deformation of the alloy sets in. However, the fracture of the 2 mm-thick specimen occurs at a much higher stress and elongation than that for the 6 and 10 mm thick specimens.
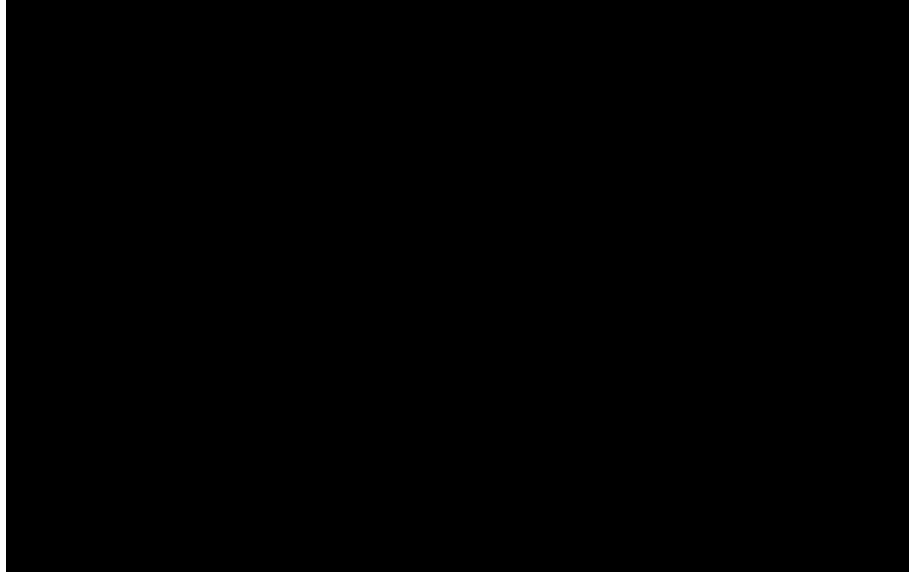
(a)
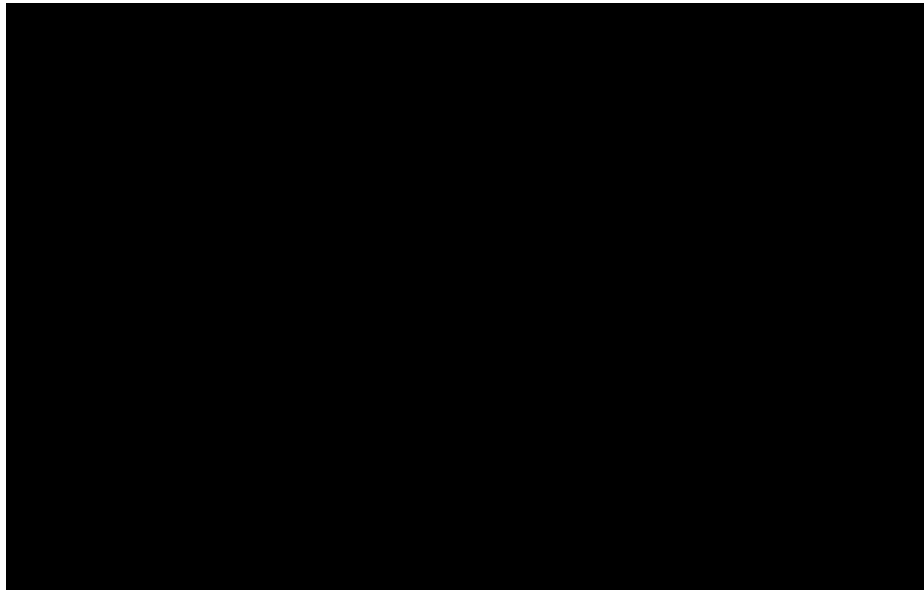
(b)
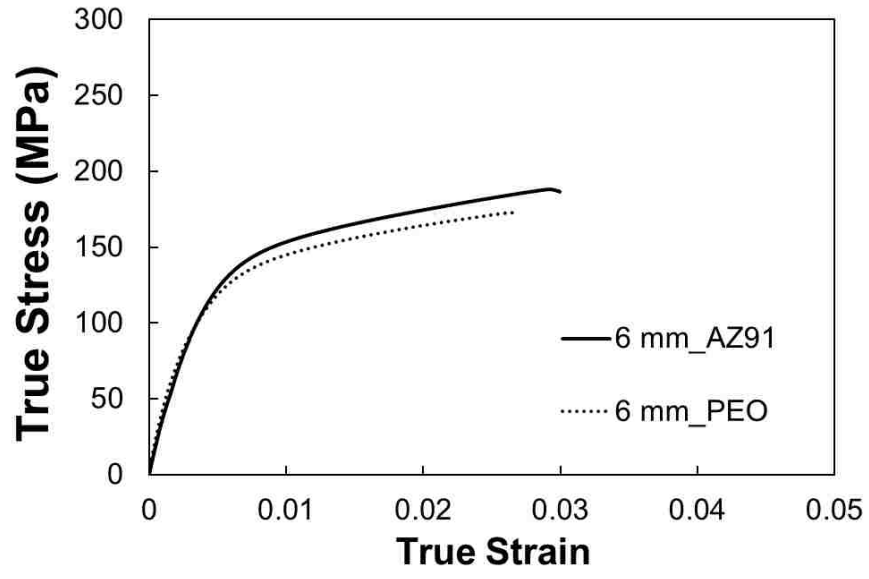
(c)

(d)

Figure 5.5 Typical true strain vs. stress curves for the die cast AZ91 alloy., (a) six curves for all three

section thickness, (b) 2 mm,(c) 6mm, and (d) 10mm.

The true stress-strain curve for metals during plastic deformation is often described by the power expression:

$$\sigma = K\varepsilon^n \qquad \text{Equation 5.3}$$

where K and n are empirical constants. The regression analysis indicates that the power expression is in a reasonable agreement with the tensile results. The numerical values of these constants in Equation 5.3 with the regression coefficients are listed in Table 5.3. Equation 5.3 can be differentiated to obtain strain-hardening rates ($d\sigma/d\varepsilon$).

Table 5.3 Best fits parameters for power equations

Section Thickness (mm)	Surface Type	K (MPa)	n	R^2
2	Uncoated	449.58±5.71	0.1776±0.0051	0.96±0.02
	PEO Coated	410.94±6.32	0.1968±0.0048	0.96±0.02
6	Uncoated	388.66±5.83	0.2039±0.0063	0.98±0.02
	PEO Coated	388.21±7.52	0.2088±0.0072	0.98±0.02
10	Uncoated	386.51±8.64	0.2208±0.0081	0.99±0.01
	PEO Coated	387.53±9.12	0.2155±0.0077	0.99±0.01

The strain-hardening behaviors of each coated die cast AZ91 alloy are illustrated in a plot of strain-hardening rate ($d\sigma/d\varepsilon$) vs true plastic strain (ε) during the plastic deformation as shown in Figure 5.6, which is derived from Figure 5.5. Based on the

strain hardening rate, even with the PEO coating, the 2 mm specimen exhibits the highest strain hardening rate, and the 10 mm specimen remains the least strain hardening rate.

The strain hardening rates at the beginning of the plastic deformation for all the uncoated and coated samples are revealed in Figure 5.6. All the six testing samples show the similar trend of strain hardening, in which the strain hardening rates decrease with the increasing true strains. The comparison between the uncoated samples at the true strain of 0.006 indicates that the 2-mm specimen has the highest strain hardening rate of 5388.86 MPa, while the 6 and 10-mm specimens have 4653.28 MPa and 4596.57 MPa, respectively. The high strain hardening rate of the 2-mm specimen should be attributed to the low porosity content, fine microstructure, and high content of intermetallic phase $Mg_{17}Al_{12}$. With the PEO coating on the HPDC AZ91 alloy, the strain hardening rate of the 2-mm specimen decreases from 5388.86 MPa to 4913.37 MPa, which gives a drop of 8%. The reduction in strain hardening rates by the application of a coating on the thin specimen might result from the fact that the pores in the coating could be the initiation sites for cracking, and discount the material capability of strengthening itself during plastic deformation. There is almost no change in strain hardening rates to the PEO coated 6 (4641.05 MPa at $\varepsilon = 0.006$) and 10-mm (4630.35 MPa at $\varepsilon = 0.006$) specimens. This suggests that a thin PEO coating of 7.5 μm has a limited influence on the strain hardening behavior of the HPDC AZ91 alloy with the relatively thick sections. Among all the uncoated and coated samples, the uncoated and coated 2-mm specimens have the strain hardening rates higher than the counterparts in the 6 and 10-mm thickness, which implies that the microstructure of the substrate plays a more important role in strain hardening than that of the thin PEO coating on the HPDC AZ91 alloy.

Overall, the PEO coating has the effect on strain hardening rates of the thin specimen more significantly than those of the thick ones. Even though the effect of PEO coating on strain hardening is obvious, it is evident that the section thickness could be a factor to determine how the PEO coating affect the mechanical properties of magnesium alloys.
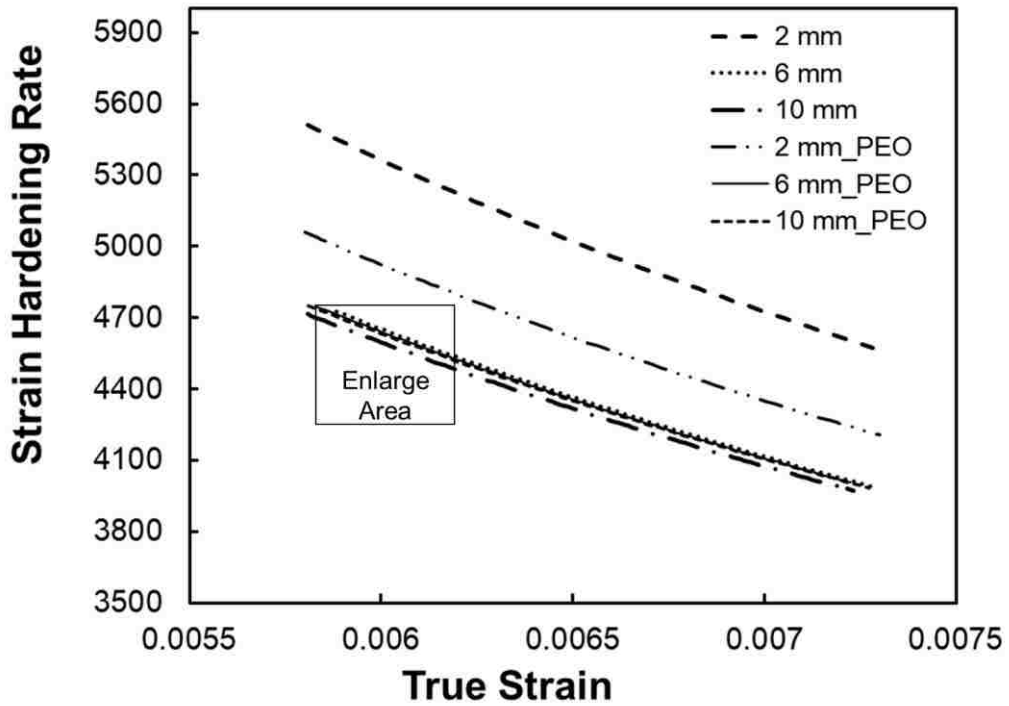
(a)
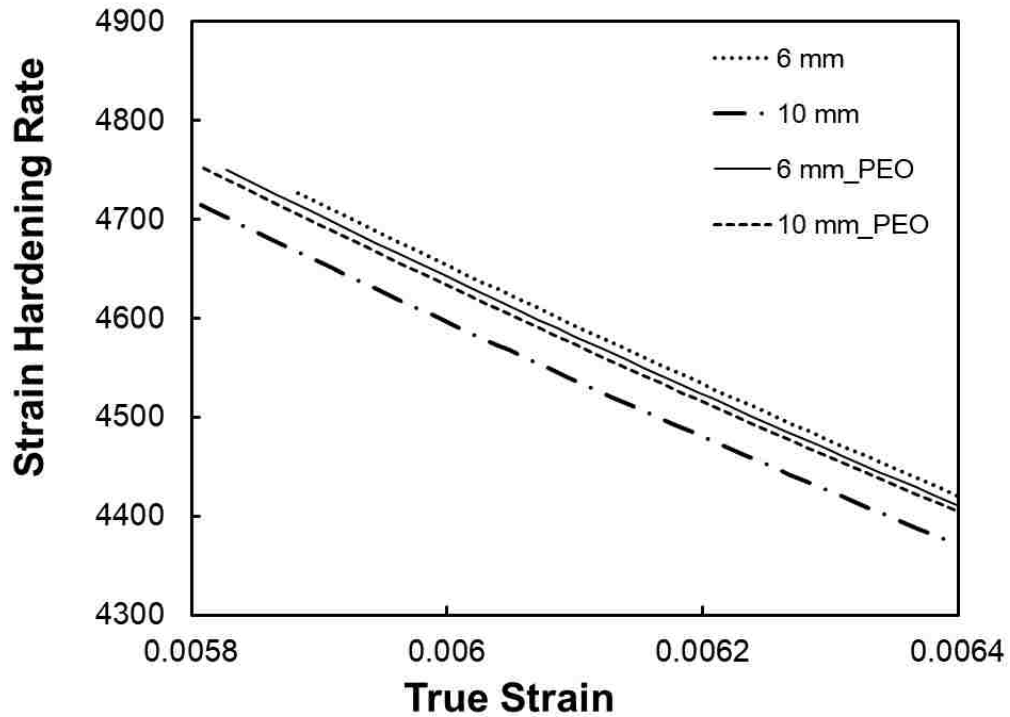
(b)

Figure 5.6 (a)Strain hardening rate vs. true strain for plastic deformation of PEO coated AZ91D alloy;

(b) Enlarge area of Strain hardening rate vs. true strain for plastic deformation

5.3.5 Fracture Behavior

Examination of the fracture surfaces of the tensile specimens via SEM manifests the

fracture behavior of PEO coated HPDC AZ91 with the three different thicknesses, which

are shown in Figures 5.7-5.9. The circled areas are observed under a high magnification

in an attempt to reveal detailed features of the fracture surface and determine the fracture

mechanism. The analysis of SEM fractography shows that the fracture behavior of PEO

coated AZ91 is influenced by the section thicknesses and the surface condition.

The fracture surface of the 2 mm thick specimen illustrated in Figure 5.7 is primarily

semi ductile in nature, which is characterized by the presence of microvoids in the shape

of cup and cone. The fractography with a high magnification, Figure 5.7 (b), portrays the microvoids with certain deformation marking along the walls of individual craters. A certain amount of energy is consumed in the process of the formation of microvoids and microvoid linkage, eventually leading to the creation of cracks. Thus, this type of fracture failure results from the coalescence of microvoids under the tensile stress. It seems, however, that the failure of the PEO coated 10 mm-thick specimen is basically caused by a combined brittle fracture mechanism of void coalescence and intergranular fracture (Figure 5.9). The fracture surface of the coated 10 mm thick specimen is reasonably smooth and flat. The low magnification SEM micrograph as shown in Figure 5.9(a) reveals the presence of river marking, which run in a direction roughly parallel to crack propagation. The local stress condition and the grain orientation might be responsible for the direction deviation. Figure 5.9 (b) with the high magnification discloses the microvoids and river marking in fact ridges, of which a few have a distinct V-shape. This observation suggests that the fracture of the coated 10 mm specimen is quasi-cleavage. Under a high tensile load, the coated specimen experiences a catastrophic failure. The similar mechanism for the fracture of die cast magnesium alloys has also been reported in reference 10.
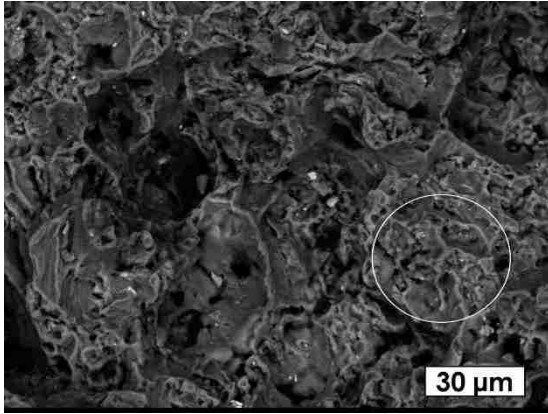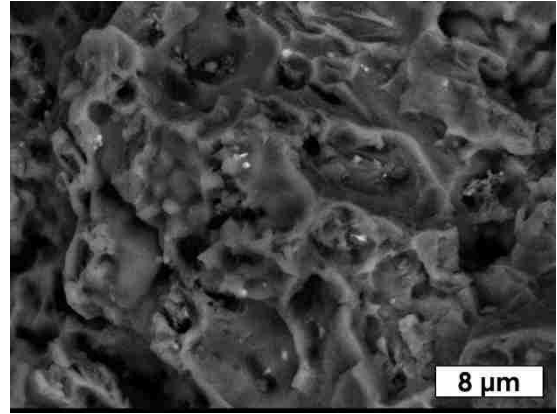
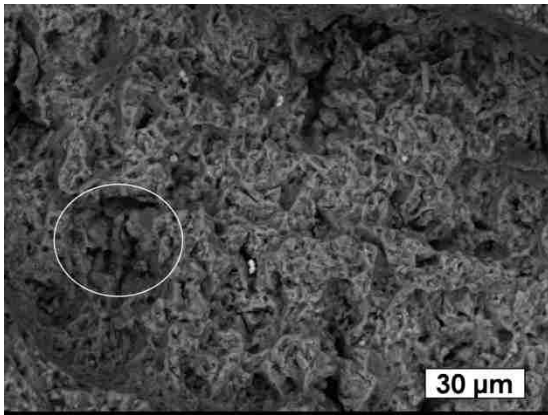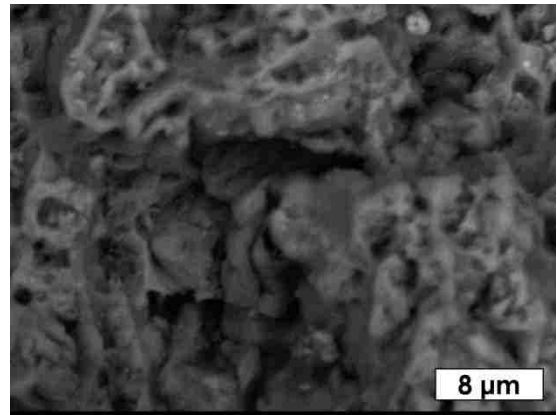(a)   (b)

Figure 5.7 SEM fractography of the PEO coated 2 mm-thick die cast coupons, (a) low and (b) high

magnifications

(a)   (b)

Figure 5.8 SEM fractography of the PEO coated 6 mm-thick die cast coupons, (a) low and (b) high

magnifications

(a)   (b)
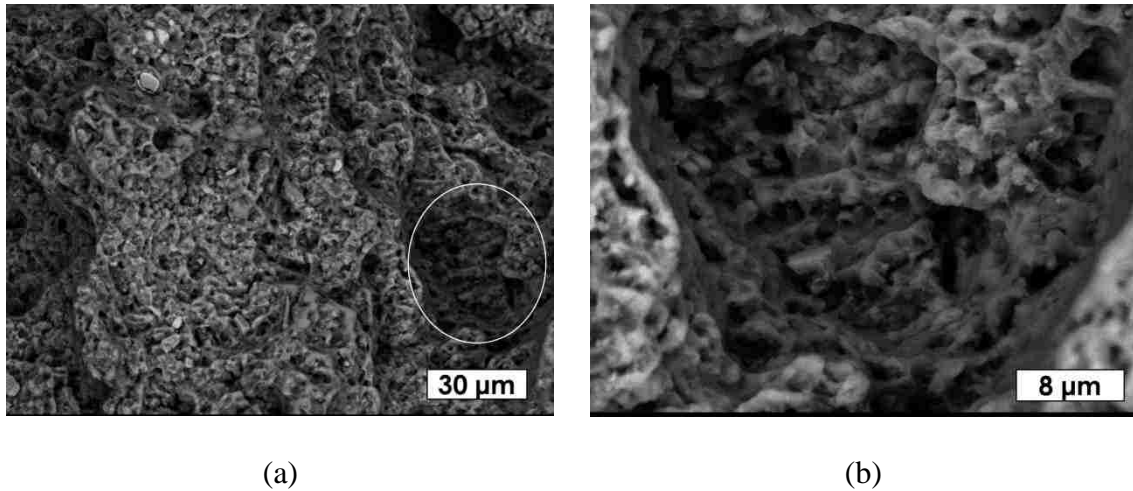
Figure 5.9 SEM fractography of the PEO coated 10 mm-thick die cast coupons, (a) low and (b) high

magnifications

A PEO process has been applied to form a protective coating on high pressure die cast AZ91 magnesium alloy. Compared with the group of the PEO coated samples, the results show the identical trend of effect by section thickness, where mechanical properties decrease with increase the section thickness. The tensile test and defamation behavior result of PEO coated follows the patterns that effect by section thickness. This implies that the low porosities, fine microstructure, and high content of intermetallic phase Mg17Al12 of AZ91 alloy samples still play an important role when the magnesium alloys are under the load.

However, in comparison between PEO coated and uncoated samples, the influence of PEO coating depends the substrate microstructure condition. For the 2 and 6 mm samples, the PEO coatings reduce the tensile properties of HPDC Mg alloy AZ91. This is due to the unmatched porosity content and microstructure size, where the outer coating layer

provides initiation sites of cracking, and consequently reduces the tensile strengths and strengthening hardening rates under tensile loading. On the other hands, for the 10 mm PEO coated samples, the PEO coating increases the tensile properties and strain hardening rate. This is because the pores in the PEO coating on the 10 mm specimen are both smaller in size and less in porosity content than those in the substrate. Thus, the ceramic layers have a limited influence on 10 mm AZ91 alloy. It is certain to conclude that the PEO coating reduces the overall mechanical properties on the thin section thickness samples which have a low porosity and fine microstructure. Yet, in the thick section thickness, the large pores and high porosity content play a dominant role in controlling mechanical properties of the HPDC Mg alloy AZ91, compare with the relatively small pores and low level of porosity present in the PEO coating.

[1] H. Hu. "Squeeze Casting of Magnesium Alloys and Their Composites", Journal of Materials Science Vol. 33, pg. 1579-1589, 1998.

[2] P. Zhang., X. Nie, H. Hu, & Y. Liu. "TEM analysis and tribological properties of Plasma Electrolytic Oxidation (PEO) coatings on a magnesium engine AJ62 alloy". Surface and Coatings Technology,Vol. 205(5), pg. 1508, 2010.

[3] Y. Ma, H. Hu, D. Northwood, & X. Nie. "Optimization of the electrolytic plasma oxidation processes for corrosion protection of magnesium alloy AM50 using the Taguchi method". Journal of materials processing technology,Vol. 182(1-3), pg. 58-64, 2007.

[4] P. B. Srinivasan, C. Blawert, & W. Dietzel. "Effect of plasma electrolytic oxidation coating on the stress corrosion cracking be haviour of wrought AZ61 magnesium alloy".Corrosion Science,Vol. 50(8), pg. 2415-2418, 2008.

[5] P. B. Srinivasan, C. Blawert, W. Dietzel, & K.U. Kainer. "Stress corrosion cracking behaviour of a surface-modified magnesium alloy".Scripta Materialia, Vol. 59(1), pg. 43-46, 2008.

[6] A. Němcová, P. Skeldon, G.E. Thompson, S. Morse, J. Čížek, & B. Pacal. "Influence of plasma electrolytic oxidation on fatigue performance of AZ61 magnesium alloy". Corrosion Science,Vol. 82, pg. 58-66, 2014.

[7] J. Hu, & X. Nie. "Effect of nanostructured oxide coatings on tensile properties of cast pure magnesium". In Advanced Materials Research, Vol. 1088, pp. 18-22, 2015.

[8] Z.Sun, , L.Ren, X. Geng, L. Fang, X. Wei, & H. Hu. "Influence of Wall Stocks on Mechanical Properties of HPDC AZ91". Key Engineering Materials, Vol. 793, pg. 41-45, 2019.

[9] H. Hu & Z. Sun : Internal Research, University of Windsor, 2019.

[10] Z. Sun, M. Zhou, N, Li, and H. Hu. "Strain-Hardening and Fracture Behavior of Die Cast Magnesium Alloy AM50", *Adv.Mater.SCI ENG,* Vol. 2007, article ID 64195, 5 pages, 2007.

The conclusions drawn from this study can be classified into two categories based on two research objectives:

I. **Effect of Section Thicknesses on Tensile Behavior and Microstructure of High Pressure Die Cast Magnesium Alloy AZ91**

1. The microstructural features of the high pressure die cast magnesium alloy AZ91 with three different section thicknesses, 2, 6 and 10 mm were studied via metallography, SEM/EDS analysis. The microstructure for all three the section thicknesses of specimens contains the primary α-Mg, β-Mg$_{17}$Al$_{12}$ intermetallics, Mn-Al phases. The intermetallic phase β-Mg$_{17}$Al$_{12}$ occupies the intergranular regions between the α-Mg grains.

2. The section thickness has a significant influence on microstructure evolution of die cast AZ91. The grain size increases with an increase in the section thickness of specimens.

3. High porosity levels and large primary α-Mg dendrites and pores are presented in die cast AZ91 with relatively thick cross-sections. The observation via SEM fractography illustrates that the fracture behavior of die cast AZ91 is influenced by section thicknesses. As the section thickness increases, the fracture of AZ91 tends to transit from ductile to brittle mode.

4. The results of tensile testing indicate that the mechanical properties, UTS, YS, and e_f, decrease significantly with an increase in the section thickness of specimens.

5. It appears that the section thicknesses determine porosity level and microstructure characteristics, and consequently dictate tensile properties of die cast magnesium alloy AZ91.

II. **Effect of Plasma Electrolytic Oxidation (PEO) on Tensile Properties of High Pressure Die Cast Magnesium Alloy AZ91**

1. The microstructure characteristics of the HPDC alloy AZ91 substrate remain the major role in determining the overall mechanical properties and tensile behavior of the uncoated and PEO coated specimens.

2. The PEO coating significantly reduces the tensile properties of the 2 mm and 6 mm section thickness samples due to the presence of porosity. With the relatively large size of pores and high content of porosities, the ceramic coating becomes the initiation sites of cracking which reduces the mechanical properties of the thin specimen.

3. The tensile properties of the 10 mm specimen slightly increase with the presence of the PEO coating. This is because the thin PEO coating contains pores smaller in size and less in content than those in the substrate, which provides protection from crack initiation and growth during tensile loading.

4. The effect of PEO coating depends on the volume fraction of the section thickness and the different level of porosities content between the substrate and the outer coating layer. High similarity of porosity content is prone to have limited effect on the tensile properties.

5. The microstructure of PEO coating on AZ91 with three different section thickness, 2, 6, and 10 mm were studied via metallography, SEM/EDS analysis. The results reveal that the strain hardening rate are insignificantly affected by the PEO coating, particularly for the 6 and 10 mm specimen samples.

This study carried out the investigation of the effect on tensile properties of different section thickness of HPDC magnesium alloy AZ91 and the effect of PEO coating on tensile properties of HPDC magnesium alloy AZ91 with different section thickness. This study laid a foundation for further investigation on finding the relation between PEO coating and the mechanical properties of magnesium and its alloys. The following are the suggestions for the future work.

- Study the effect of different thicknesses of PEO coating on mechanical properties of one specific section thickness (recommended on 10 mm) of magnesium alloy AZ91, examine their microstructure in the coating layer and substrate

- Analyze the effect of volume fraction of PEO ceramic coating affects the mechanical properties of magnesium alloy AZ91

- Investigate the effect of different electrolyte compositions on PEO coating thicknesses, which might resulted in the effect on the mechanical properties of magnesium alloy

- Investigate the correlation between the specimen thickness, the PEO coating layer thickness, and the tensile properties, which could result in an optimal combination to maximize the mechanical properties.

NAME: Zixi Sun

PLACE OF BIRTH: Moscow, Russia

YEAR OF BIRTH: 1993

EDUCATION: Windermere Preparatory School, Orlando, FL, 2013

                            University of Windsor, B.Sc., Windsor, ON, 2017

                            University of Windsor, M.Sc., Windsor, ON, 2019